CHAPTER 17

DETACHMENT PROCESSES FOR MOLECULAR ANIONS

Jack Simons*
Chemistry Department University of Utah
Salt Lake City, Utah 84112

Contents

---

*Henry Eyring Center for Theoretical Chemistry.

1. Introduction

1.1. *Scope of this Chapter*

In this chapter, I will attempt to describe the theory underlying electron detachment in molecular anions, including detachment induced by photon absorption (photodetachment) and by energy transfer from rotational, vibrational, or collisional motion. I will not attempt to review or even summarize all of the calculations of detachment rates that have been carried out on particular molecular anions, but I will discuss some of the more recent areas of research that I believe offer fruitful lines of pursuit. For the reader who is interested in gaining an overview of what is known experimentally and theoretically about molecular anions, several review articles, books, and other sources[1–9] can be recommended. Most of these sources focus on the nature of the electronic structure of anions rather than on how such species undergo electron detachment; therefore, I believe the present chapter is timely and hopefully informative.

1.2. *Various Stabilities of Molecular Anions*

Let me begin by making it clear what it means for a molecular anion to be electronically stable, locally geometrically stable, and thermodynamically

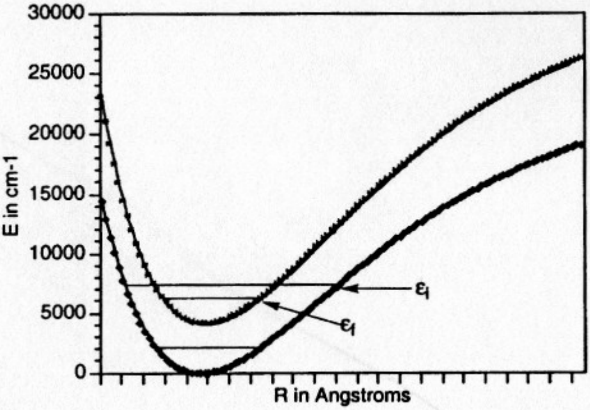

Fig. 1. Anion (lower) and neutral (upper) potential energy surfaces as functions of internuclear distance R illustrative of the ground states of NH^- and NH.

stable. A clear understanding of these terms is important for the discussion provided in this chapter.

1.2.1. *Electronically Stable*

If, at a fixed molecular geometry (whose internal coordinates are denoted $\mathbf{Q} = Q_1, Q_2, \ldots, Q_{3N-6}$ for a nonlinear molecule with N atoms), the anion's electronic energy is lower than that of the neutral molecule at this same geometry, the anion is said to be *electronically stable* at this geometry. Figure 1 shown below illustrates the electronic energies of the ground states of the NH^- anion[10] and its neutral counterpart NH as functions of the internuclear distance R. This anion is electronically stable over all internuclear distances displayed.

Figure 2 shows the ground state anion and neutral energies typical of enolate anions[11] as functions of the rotation about the C–C bond axis. In this case, the anion is electronically stable for the range of angles shown.

Figure 3 shows anion and neutral energy curves characteristic of an anion that is electronically stable over geometries accessed by its low-energy vibrational levels but is electronically unstable at other geometries.

1.2.2. *Locally Geometrically Stable*

If, at a specific geometry $\mathbf{Q}^0$, (1) the anion is electronically stable and (2) the anion's electronic energy $E(Q_i)$ as a function of displacements δQ_i away

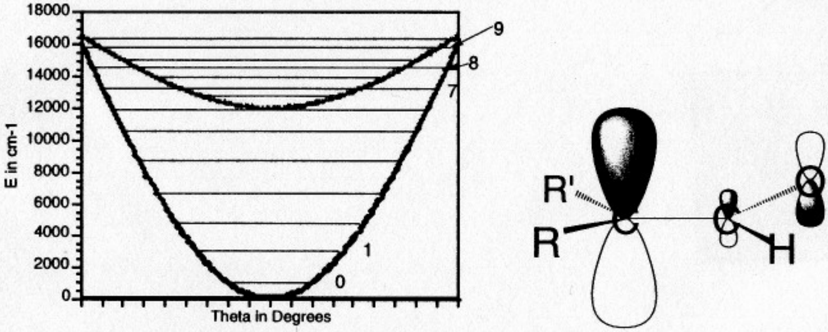

Fig. 2. Anion (lower) and neutral (upper) potential energy surfaces illustrative of enolate anions (shown at right) as functions of the torsion angle about the C–C bond axis.

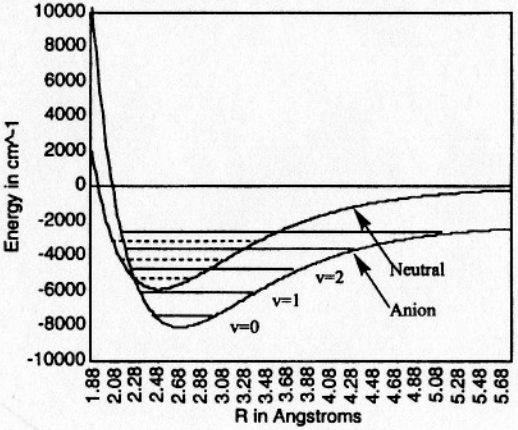

Fig. 3. Anion and neutral curves as functions of bond length for a case where the anion is electronically stable over a limited range of geometries.

from Q_i^0 obeys

$$\partial E/\partial Q_i = 0, \text{ for all } i \text{ and}$$

the square Hermitian–Hessian matrix $\partial^2 E/\partial Q_i \partial Q_j$ has all $3N-6$ eigenvalues positive, then the geometry $\mathbf{Q}^0$ corresponds to a local minimum on the anion's energy surface. In such situations, we say that this geometry of the anion is locally (i.e. near $\mathbf{Q}^0$) geometrically stable. The NH^- anion shown in Fig. 1 and the enolate anion shown in Fig. 2 are geometrically stable at their equilibrium bond length and equilibrium angle, respectively.

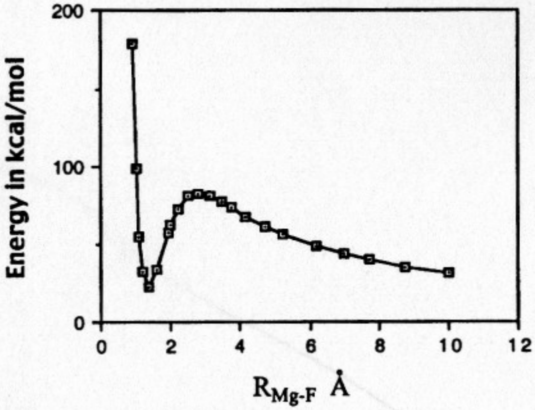

Fig. 4. Energy of MgF_4^{2-} as a function of one Mg–F bond length with all other degrees of freedom optimized (taken from Ref. 12). The energy of $MgF_3^- + F^-$ (at $R \to \infty$) is defined as zero.

1.2.3. *Thermodynamically Stable*

An anion is thermodynamically stable if it is electronically and geometrically stable and if its energy at its lowest-energy structure lies below that of any molecular or atomic fragments into which it might dissociate.

The NH^- anion is thermodynamically stable because, at its lowest-energy structure, its energy is lower than the energy of $H^- + N$ or $N^- + H$. Figure 4 shows the electronic energy of the MgF_4^{-2} dianion[12] as a function of one Mg–F bond length (with the remaining three Mg–F bond lengths and all internal angles "optimized" to minimize the energy).

This dianion is geometrically stable near $R = 1.7$ Å, and is electronically stable (i.e. MgF_4^{2-} lies below MgF_4^- plus a free electron). However, this dianion is not thermodynamically stable because its energy near $R = 1.7$ Å lies above the energy of $MgF_3^- + F^-$ by ca. 20 kcal/mol.

1.3. *Various Mechanisms for Molecular Anions to Eject an Electron*

Let us consider a molecular anion that is vibrating (and rotating) in the neighborhood of one of the local minima on its energy surface and that is electronically stable over the range of geometries accessed by these motions (including tunneling). This anion has no way to eject an electron without the input of energy from an external sources. Hence, it can exist in this state indefinitely. The lowest vibrational level of the NH^- anion shown in Fig. 1 as well as the $v = 0$ through $v = 6$ torsional levels of the enolate of Fig. 2 present examples of molecular anion states that cannot undergo detachment in the absence of some external perturbation.

Given an anion in a state that is stable to detachment as discussed above, there are two primary tools that are commonly employed to cause the anion to eject an electron:

1. One or more *photons* can be used to induce an *electronic excitation* of the anion to a final state in which an electron exists in a continuum orbital rather than in a bound orbital. Alternatively, the photon(s) may cause *excitation* of the anion's *vibrational/rotational modes* to an extent that the anion's total (electronic plus vibrational/rotational) energy lies above one or more levels of the neutral molecule. The upper vibrational levels of NH^- shown in Fig. 1 and enolate torsional levels higher than $v = 6$ shown in Fig. 2 offer examples of this situation.
2. *Collision* with an atom, molecule, or other particle projectile (e.g. cation, anion, or electron) can induce either an *electronic excitation* in the anion to a final continuum state or an *excitation of* the anion's *vibrational and/or rotational modes.*

1.3.1. *Direct Photon-Initiated Detachment*

In the photon-induced electronic transition process, if the final electronic state of the anion is electronically unstable relative to one or more states of the neutral molecule, one achieves what is termed a *direct photodetachment* event. This process can be viewed as an electronic transition connecting an electronically bound state (the anion) to an electronically unbound state (the neutral plus ejected electron system). The theory behind this family of detachment processes is treated in Sec. 2 and is very similar to the theory of molecular photoionization treated by Berrah elsewhere in this book.[13] An example of such transitions is given in Fig. 5 where $v = 0 \to v = 0, 1, 2$ transitions in $NH^- \to NH + e^-$ are illustrated.[10]

1.3.2. *Photon-Initiated Detachment Involving Non-Born–Oppenheimer Coupling*

Alternatively, one or not more photons may induce vibration/rotation excitation of the anion to a final level that lies above one or more levels of

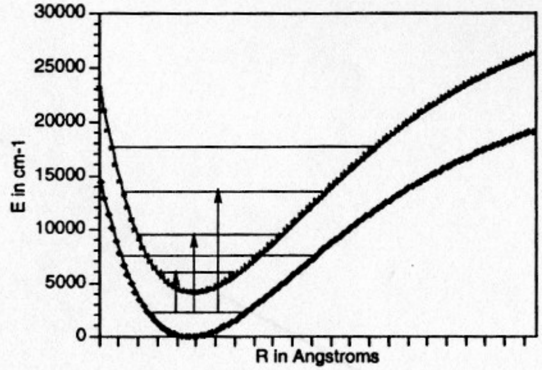

Fig. 5. Direct photodetachment from $v = 0$ NH$^-$ to $v = 0, 1, 2$ of NH + e^-.

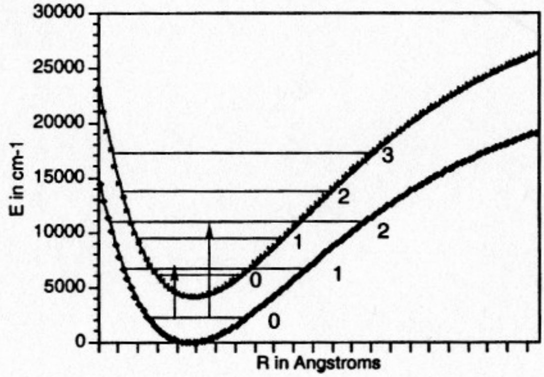

Fig. 6. Vibrational excitation of NH$^-$ from $v = 0$ to $v = 1, 2$.

the neutral molecule. In Fig. 6, a case in which NH$^-$ is excited from the $v = 0$ of its ground electronic state to $v = 1$ or $v = 2$ of this same electronic state is illustrated. In this situation, the $v = 1$ anion state may undergo subsequent electron detachment to the $v = 0$ level of NH by ejecting an electron with kinetic energy equal to the $v = 1$ NH$^-$ to $v = 0$ NH energy gap. The $v = 2$ level of NH$^-$ can decay to either $v = 1$ NH or $v = 0$ NH ejecting an electron of the appropriate kinetic energy.

The theory underlying this kind of electron detachment is covered in Sec. 3. Briefly, the photon absorption step is described by the conventional theory of infrared (when vibrational excitation is involved) absorption as discussed in a variety of spectroscopy text books.[14,15] Once the anion is vibrationally and/or rotationally excited, it must convert some or all of its excess vibrational/rotational energy into electronic energy to eject an electron. The origin of this energy transfer lies in the dynamical couplings that are ignored when the Born–Oppenheimer (BO) approximation[16] is made. Such non-BO induced electron ejection rates are treated in Sec. 3.2.

1.3.3. *Photon-Initiated Detachment Involving Shape and Feshbach Resonances*

In addition to the case discussed above in which vibration/rotation energy must be converted to electronic energy, excitation to higher vibrational levels of the anion can induce electron ejection by causing the anion to sample geometries where the anion's electronic energy lies above that of the neutral. Such a case is illustrated in Fig. 3. For this species, the lower anion vibrational levels do not sample geometries where the anion is electronically unstable (at least in the absence of great tunneling). In contrast, from $v = 2$ onward, the vibrational motion samples regions of electronic instability for the anion; within such regions, an electron can be ejected spontaneously (i.e. without any energy input from photons or via coupling to vibrational/rotational energy). The rate at which electrons are detached in such cases is determined by two factors: (1) the frequency with which vibrational motion causes such regions of spontaneous instability to be accessed, and (2) the rate at which an electron is detached within these regions. The former rate is simply the rate of vibrations along coordinates that move the system into the regions of instability. The latter rate depends strongly upon the nature of the electronic transition[17] that occurs when the anion spontaneously loses its "extra" electron.

1.3.3.1. *Shape Resonances*

Specifically, if the occupancy of spin-orbitals in the anion (which we denote $\phi_1\phi_2\cdots\phi_L\phi_K\phi_N$) differs from that in the neutral molecule produced in the detachment by the *loss of a single spin-orbital* (e.g. ϕ_N), and if the spin-orbital ϕ_N has no spherical character (i.e. if it contains only p, d, or higher angular momentum character, but no s-character), then the ejection rate is governed by the rate at which the electron tunnels through an angular momentum barrier. States that decay through such single-spin-orbital electron tunneling detachments are called *shape resonance* states, and they usually have decay rates in the range of 10^{14}–10^{16} sec^{-1}.

The N_2^- anion in which the "extra" electron has attached to the π_g^* antibonding orbital of N_2 offers an example of a shape resonance, as does the ethylene anion $H_2C{=}CH_2^-$ in which the electron occupies the π^* C–C orbital. In both cases, the fact that the orbital occupied by the extra electron possesses (at least) one nodal plane precludes its having any spherical character. At long range from the underlying neutral's nuclei and other electrons, the electron in the anion's highest occupied molecular orbital (HOMO) experiences an attraction to the neutral determined by a potential $V(\mathbf{r})$. This potential can be expanded in terms of spherical harmonics to display its angular and radial character (the angles θ and ϕ and the radial coordinate r describe the position of the electron $\mathbf{r}$ in a coordinate system fixed to the molecule)

$$V(\mathbf{r}) = \Sigma_{L,M} Y_{L,M}(\theta,\phi) V_{L,M}(r)\,.$$

This expansion posesses no $L = 0$ character because the anion's HOMO has a nodal plane. For N_2^-, its largest term would involve $L = 2$ because the π_g^* orbital, as shown below, clearly has strong d-character when expanded about the center of the N–N bond.

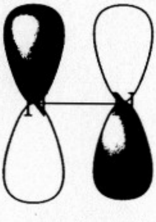

Fig. 7. The anti-bonding π^* orbital of N_2^-.

For CO^-, the anti-bonding π^* orbital clearly possesses both $L = 1$ and $L = 2$ character as shown in Fig. 8.

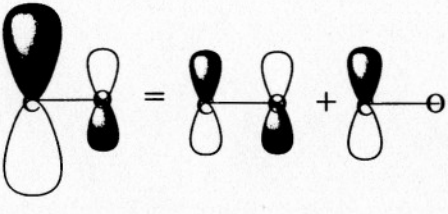

Fig. 8. The anti-bonding π^* orbital of CO^- expressed as a sum of $L = 2$ and $L = 1$ components.

When the expansion for $V(\mathbf{r})$ and a similar expansion of the wavefunction $\psi(r, \theta, \phi)$

$$\psi(\mathbf{r}) = \Sigma_{L,M} Y_{L,M}(\theta, \phi)\psi_{L,M}(r)$$

are used in the Schrödinger equation,

$$-\hbar^2/2m_e \partial/\partial r(r^2 \partial\psi/\partial r) + L^2/2m_e r^2 \psi + V(\mathbf{r})\psi = E\psi$$

a set of coupled equations is obtained for the wavefunction amplitudes $\psi_{L,M}(r)$. When there exists a single dominant $V_{L,M}(r)$ as in the case of N_2^- (where $L = 2$ dominates), the equation for the corresponding wavefunction amplitude is

$$\begin{aligned}&-\hbar^2/2m_e \partial/\partial r(r^2 \partial\psi_{L,M}/\partial r)\\ &\qquad + L(L+1)/2m_e r^2 \psi_{L,M} + V_{L,M}(r)\psi_{L,M} = E\psi_{L,M}\,.\end{aligned}$$

Depicted in Fig. 9 are the effective radial potentials $V_{\text{eff}}(r) = V(r) + L(L+1)/2m_e r^2$ for hypothetical cases with different L values.

The centrifugal potential $L(L+1)2m_e r^2$ has two effects on the decay rate of a shape resonance state. First, it moves the energy of the state to a higher value than the energy in the Schrödinger equation with the same $V(r)$ but with no centrifugal potential. This tends to destabilize the anion

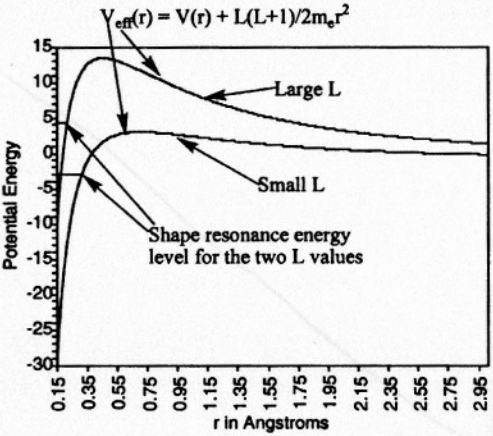

Fig. 9. The effective radial potential experienced by an electron in an orbital having angular momentum L and attracted to the underlying molecule by a potential $V(r)$.

and thus increase its decay rate. Second, the centrifugal potential provides the "barrier" through which the electron must tunnel to detach, this, of course, tends to decrease the decay rate as L increases. The net result of both effects is illustrated above in Fig. 9. Some molecular anions display a large number of shape resonance states having different L values; the pattern of decay rates of these states as functions of L is often complicated by these two competing effects of the centrifugal potential.

1.3.3.2. *Feshbach Resonances*

When the anion's spin-orbital occupancy differs from that of the daughter neutral by *two spin–orbitals* (e.g. if ϕ_N were lost to produce the ejected electron in the continuum orbital ϕ_C and ϕ_L were excited to a spin-orbital ϕ_X not present in the anion), the ejection rate is governed by the strength of coupling between the two configurations $\phi_1\phi_2\cdots\phi_L\phi_K\phi_N$ and $\phi_1\phi_2\cdots\phi_X\phi_K\phi_C$. The coupling V, induced by the electronic Hamiltonian H, between these two configurations can be expressed in terms of the two-electron integrals:

$$V = \int d\mathbf{r} \int d\mathbf{r}' \phi_C(\mathbf{r})\phi_X(\mathbf{r}')e^2/|\mathbf{r}-\mathbf{r}'|\{\phi_N(\mathbf{r})\phi_L(\mathbf{r}') - \phi_L(\mathbf{r})\phi_N(\mathbf{r}')\}\,.$$

States that decay in this manner are called *Feshbach resonance* states, and they usually have smaller electron ejection rates (ca. 10^{13}–10^{15} $\sec^{-1}$) than do shape resonance states. The state of N_2^- in which an electron is attached to the anti-bonding π_g^* orbital and a second electron is excited from a non-bonding σ_g orbital into the π_g^* orbital provides an example of a Feshbach resonance state. To eject an electron, this state must undergo a two-electron rearrangement whose rate is determined by the square of the two-electron integral

$$V = \int d\mathbf{r} \int d\mathbf{r}' \phi_C(\mathbf{r})\sigma_g(\mathbf{r}')e^2/|\mathbf{r}-\mathbf{r}'|\pi_g^*(\mathbf{r})\pi_g^*(\mathbf{r}')$$

multiplied by the density of translational states ρ for the ejected electron.

1.3.4. *Collision-Induced Detachment*

Collision of an electronically stable anion with another species can cause electron ejection by most of the mechanisms enumerated above when photons are involved. That is, the collision can simply replace the photon in exciting the stable anion to an excited electronic state or to an excited vibration/rotation state which, subsequently, can detach an electron via non-BO coupling or by accessing geometries where the anion becomes electronically unstable to decay (via shape or Feshbach mechanism). The theory underlying collision-induced detachment is similar to that governing the photon-initiated events except for the rates and selection rules that deal with the initial energy transfer process (i.e. the photon absorption or the collisional excitation).

Before closing this Introduction, I should mention that there are molecular anions that do not lie within the scope of this chapter. Specifically, some molecular anions do not possess any range of geometries over which (1) the anion is electronically stable and (2) the anion potential energy surface has a local minimum deep enough to support one or more bound vibrational levels. In this chapter, attention is restricted to those anions that can exist as electronically and locally geometrically stable units which thus are amenable to identification and isolation (e.g. by mass selection) and which must subsequently be excited by photons or collisions to induce electron detachment. The detachment can take place by (1) direct photon excitation of the electronic degrees of freedom, (2) excitation of vibration/rotation modes followed by non-BO excitation of the electrons, or (3) excitation of vibration/rotation modes causing structural deformation into geometries where the anion is electronically unstable and thus may decay as a shape or Feshbach resonance. An example of an anion that does not have an electronically and geometrically stable state is shown in Fig. 10.

I have chosen not to examine such anions (i.e. those that exist only as resonances and have no electronically and geometrically stable states) in this chapter because (1) their experimental study involves entirely different tools than are characteristic of this Book, (2) their theoretical study is highly specialized and (3) both the experimental and theoretical aspects of their study have been reviewed in the not too distant past.[1,3]

2. Direct Photodetachment

An electronically and locally geometrically stable molecular anion interacts with the electromagnetic field of a photon source much as a neutral molecule does. The primary difference between photoionization of a neutral and photodetachment of an anion lies in the form of the wavefunction describing the ejected electron. These differences are detailed further below.

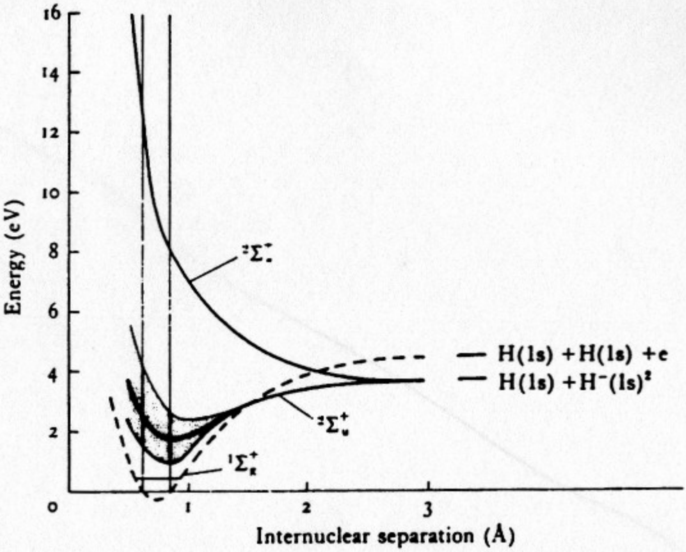

Fig. 10. Energy curves similar to those of ground state $X^1\Sigma_g^+$ H_2 and the lowest H_2^- state.

2.1. *Time Dependent Perturbation Rate Expression*

The theory used to obtain expressions for rates of electron detachment proceeds as follows.[18] First, the interaction of anion's electrons (labeled j) and nuclei (labeled a, having charges Z_a) with the vector potential $\mathbf{A}$

$$H_{\text{int}} = \Sigma_j\{(ie\hbar/m_e c)\mathbf{A}(r_j,t) \bullet \nabla_j + (e^2/2m_e c^2)|\mathbf{A}(r_j,t)|^2\}$$
$$+ \Sigma_a\{(iZ_a e\hbar/m_a c)\mathbf{A}(R_a,t) \bullet \nabla_a + (Z_a^2 e^2/2m_a c^2)|\mathbf{A}(R_a,t)|^2\}$$

is used as a perturbation in the time-dependent Schrödinger equation

$$i\hbar\partial\Psi/\partial t = (H^0 + H_{\text{int}})\Psi\,.$$

An order-by-order expansion of the wavefunction

$$\Psi = \Psi^0 + \Psi^1 + \Psi^2 + \Psi^3 + \cdots\,,$$

is combined with a realization that H_{int} has both first- and second- order components

$$H_{\text{int}}^1 = \Sigma_j\{(ie\hbar/m_e c)\mathbf{A}(r_j,t) \bullet \nabla_j\} + \Sigma_a\{(iZ_a e\hbar/m_a c)\mathbf{A}(R_a,t) \bullet \nabla_a\}$$
$$H_{\text{int}}^2 = \Sigma_j\{(e^2/2m_e c^2)|\mathbf{A}(r_j,t)|^2\} + \Sigma_a\{(Z_a^2 e^2/2m_a c^2)|\mathbf{A}(R_a,t)|^2\}\,.$$

The first-order wavefunction Ψ^1 is expanded in terms of the zeroth-order wavefunctions, which are the eigenstates $\{\Phi_f\}$ of the anion including those states lying in the continuum (i.e. corresponding to a neutral molecule and a free electron).

$$\Psi^1 = \Sigma_f D_f(t)\Phi_f \exp(-iE_f^0 t/\hbar) .$$

When used in the first-order Schrödinger equation and assuming that at $t = 0$ (just prior to when the photon field is turned on) the anion is in the electronically and geometrically stable state Φ_i having energy E_i^0, one obtains equations for the amplitudes $D_f(t)$:

$$i\hbar\partial D_f^1/\partial t = \langle\Phi_f|H_{\text{int}}^1|\Phi_i\rangle \exp(i[E_f^0 - E_i^0]t/\hbar) .$$

Using the expression for the first-order perturbation given earlier

$$H_{\text{int}}^1 = \Sigma_j\{(ie\hbar/m_e c)\mathbf{A}(r_j,t) \bullet \nabla_j\} + \Sigma_a\{(iZ_a e\hbar/m_a c)\mathbf{A}(R_a,t) \bullet \nabla_a\}$$

and writing explicitly the time- and space-dependence of the vector potential

$$2\mathbf{A}_0 \cos(\omega t - \mathbf{k} \bullet \mathbf{r}) = \mathbf{A}_0\{\exp[i(\omega t - \mathbf{k} \bullet \mathbf{r})] + \exp[-i(\omega t - \mathbf{k} \bullet \mathbf{r})]\} ,$$

gives the following expression for the D_f amplitudes:

$$\begin{aligned} D_f^1(T) = (i\hbar)^{-1}\{&\langle\Phi_f|\Sigma_j\{(ie\hbar/m_e c)\exp[-i\mathbf{k} \bullet \mathbf{r}_j]\mathbf{A}_0 \bullet \nabla_j \\ &+ \Sigma_a(iZ_a e\hbar/m_a c)\exp[-i\mathbf{k} \bullet \mathbf{R}_a]\mathbf{A}_0 \bullet \nabla_a|\Phi_i\rangle\} \\ &\times [\exp(i(\omega + \omega_{ff,i})T - 1]/i(\omega + \omega_{f,i}) \\ &+ (i\hbar)^{-1}\{\langle\Phi_f|\Sigma_j\{(ie\hbar/m_e c)\exp[i\mathbf{k} \bullet \mathbf{r}_j]\mathbf{A}_0 \bullet \nabla_j \\ &+ \Sigma_a(iZ_a e\hbar/m_a c)\exp[i\mathbf{k} \bullet \mathbf{R}_a]\mathbf{A}_0 \bullet \nabla_a|\Phi_i\rangle\} \\ &\times [\exp(i(-\omega + \omega_{ff,i})T - 1]/i(-\omega + \omega_{f,i}) , \end{aligned}$$

where $\omega_{f,i} = [E_f^0 - E_i^0]/\hbar$.

Introducing the short-hand for the non-time-dependent part

$$\begin{aligned} \alpha_{f,i} = \langle\Phi_f|\Sigma_j\{&(e/m_e c)\exp[-i\mathbf{k} \bullet \mathbf{r}_j]\mathbf{A}_0 \bullet \nabla_j \\ &+ \Sigma_a(Z_a e/m_a c)\exp[-i\mathbf{k} \bullet \mathbf{R}_a]\mathbf{A}_0 \bullet \nabla_a|\Phi_i\rangle \end{aligned}$$

allows D_f^1 to be written as

$$D_f^1(T) = \{\alpha_{f,i}[\exp(i(\omega + \omega_{ff,i})T - 1]/i(\omega + \omega_{f,i})$$
$$+ \alpha^*_{f,i}[\exp(i(-\omega + \omega_{ff,i})T - 1]/i(-\omega + \omega_{f,i})\}\,.$$

The second term in this expression is the one that has the potential of displaying "resonance character" because its denominator can approach zero as ω approaches $\omega_{f,i}$, which is a positive quantity.

Retaining only the resonant component, the modulus squared $|D_f|^2$ gives the *probability* of finding the anion in the state Φ_f at time $T > 0$:

$$|D_f^1(T)|^2 = 2|\alpha_{f,i}|^2[1 - \cos((\omega - \omega_{f,i})T)]/(\omega - \omega_{f,i})^2$$
$$= 4|\alpha_{f,i}|^2[\sin^2(1/2(\omega - \omega_{f,i})T)]/(\omega - \omega_{f,i})^2\,.$$

The quantity $[\sin^2(1/2(\omega - \omega_{f,i})T)]/(\omega - \omega_{f,i})^2$ has the ω-dependence shown in Fig. 11; the width decreases and the peak height increases as the time of interaction T with the electromagnetic field grows.

The above expression for the probability of transitions from Φ_i to Φ_f has to be modified in two ways before it is explicitly pertinent to the photodetachment case. First, it must be realized that any experimental light source does not subject the anion to a perfectly monochromatic perturbation. Even lasers produce a distribution of frequencies which is usually characterized by a so-called line-shape function $g(\omega)$. As a result, the correct

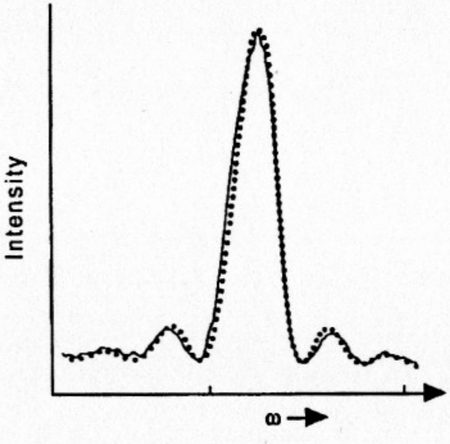

Fig. 11. Plot of $[\sin^2(1/2(\omega - \omega_{f,i})T)]/(\omega - \omega_{f,i})^2$ vs ω for one particular value of T (taken from Simons and Nichols book listed in Ref. 18).

equation for the probability of transitions averaged over the distribution of frequencies presented by the light source is

$$|D_f^1(T)|^2_{\text{ave}} = 4|\alpha_{f,i}|^2 \int g(\omega)[\sin^2(1/2(\omega - \omega_{f,i})T)]/(\omega - \omega_{f,i})^2 d\omega$$

$$= 2|\alpha_{f,i}|^2 T \int g(\omega)$$

$$\times [\sin^2(1/2(\omega - \omega_{f,i})T)]/[1/4(\omega - \omega_{f,i})^2 T^2]\, d(T\omega/2)\,.$$

The latter form of the equation is used for the following reason. If the light source's $g(\omega)$ profile is relatively constant over the narrow range of frequencies where the $[\sin^2(1/2(\omega - \omega_{f,i})T)]/(\omega - \omega_{f,i})^2$ function plotted in Fig. 11 is "peaked" (which will be the case if T is long enough), $g(\omega)$ can be approximated by $g(\omega_{f,i})$ and factored out of the integral and the identity $\int \sin^2(x)/x^2 dx = \pi$ can be used:

$$|D_f^1(T)|^2_{\text{ave}} = 2|\alpha_{f,i}|^2 T g(\omega_{f,i})$$

$$\times \int [\sin^2(1/2(\omega - \omega_{f,i})T]/[1/4(\omega - \omega_{f,i})^2 T^2]\, d(T\omega/2)$$

$$= 2g(\omega_{f,i})|\alpha_{f,i}|^2 T \int \sin^2(x)/x^2 dx = 2\pi g(\omega_{f,i})|\alpha_{f,i}|^2 T\,.$$

2.2. *The Rate and Cross-Section*

The *rate* at which transitions occur is obtained by taking the time derivative of this probability

$$R = 2\pi g(\omega_{f,i})|\alpha_{f,i}|^2$$

this gives the number of transitions per second. If one wants the *cross-section*, one divides this rate by the intensity I (number of photons per cm^2 per sec) of the light source

$$\sigma = 2\pi g(\omega_{f,i})|\alpha_{f,i}|^2/I$$

which has units of cm^2.

The second necessary modification of the rate (and cross-section) expression is to introduce the fact that the final state Φ_f is not a discrete state but, rather, is member of a continuum of states. In particular, the neutral plus ejected electron final state wavefunction is characterized by the momentum $\mathbf{p}$ (having magnitude p and orientation angles α and β relative to a molecule-fixed coordinate system) and the kinetic energy $E = p^2/2m_e$ of the ejected electron. The density of states (number of states per unit energy) for the ejected electron is

$$\rho(E) = 4\pi m_e L^3 (2m_e E)^{1/2}/\hbar^2 .$$

Introducing this density into the above expressions for the rate and cross-section gives the following expression appropriate to the photodetachment process:

$$R = 2\pi \int g(\omega_{E,i}) |\alpha_{E,i}|^2 \rho(E)\, dE$$

$$\sigma = 2\pi/I \int g(\omega_{E,i}) |\alpha_{E,i}|^2 \rho(E)\, dE$$

where the index f has been replaced by the label E because the final state Φ_f is more appropriately labeled Φ_E according to the kinetic energy of the ejected electron.

The next step in deriving more explicit expressions for photodetachment from molecular anions is to introduce the so-called long wavelength approximation into the expression for the $\alpha_{E,i}$ matrix element

$$\alpha_{E,i} = \langle \Phi_E | \Sigma_j (e/m_e c) \exp[-i\mathbf{k} \bullet \mathbf{r}_j] \mathbf{A}_0 \bullet \nabla_j + \Sigma_a (Z_a e/m_a c) \exp[-i\mathbf{k} \bullet \mathbf{R}_a] \mathbf{A}_0 \bullet \nabla_a | \Phi_i \rangle$$

and to keep only the electric dipole terms. The factors $\exp[-i\mathbf{k} \bullet \mathbf{r}_j]$ and $\exp[-i\mathbf{k} \bullet \mathbf{R}_a]$ are expanded as:

$$\exp[-i\mathbf{k} \bullet \mathbf{r}_j] = 1 + (-i\mathbf{k} \bullet \mathbf{r}_j) + 1/2(-i\mathbf{k} \bullet \mathbf{r}_j)^2 + \cdots$$

$$\exp[-i\mathbf{k} \bullet \mathbf{R}_a] = 1 + (-i\mathbf{k} \bullet \mathbf{R}_a) + 1/2(-i\mathbf{k} \bullet \mathbf{R}_a)^2 + \cdots$$

where $|\mathbf{k}| = 2\pi/\lambda$. Because the photon's wavelength λ is usually much longer than the dimensions of the molecular anion, $\mathbf{k} \bullet \mathbf{r}_j$ and $\mathbf{k} \bullet \mathbf{R}_a$ are less than unity in magnitude. If only the terms linear in $|\mathbf{k}|$ are retained, one obtains what is called the electric-dipole approximation to the transition matrix elements:

$$\alpha_{E,i} = \langle \Phi_E | \Sigma_j (e/m_e c) \mathbf{A}_0 \bullet \nabla_j + \Sigma_a (Z_a e/m_a c) \mathbf{A}_0 \bullet \nabla_a | \Phi_i \rangle$$

which can also be expressed in the so-called "length" form (rather than the "velocity" operator form shown above)

$$\begin{aligned}\alpha_{E,i} &= \omega_{E,i}\mathbf{A}_0 \bullet \langle\Phi_f|\Sigma_j(e/\hbar c)\mathbf{r}_j + \Sigma_a(Z_a e/\hbar c)\mathbf{R}_a|\Phi_i\rangle \\ &= (\omega_{E,i}/\hbar c)\mathbf{A}_0 \bullet \langle\Phi_f|\mu|\Phi_i\rangle\end{aligned}$$

where μ is the electric dipole moment operator for the electrons and nuclei:

$$\mu = \Sigma_j e\mathbf{r}_j + \Sigma_a Z_a e\mathbf{R}_a\,.$$

Within this approximation, the overall rate of transitions is given by:

$$\begin{aligned}R &= 2\pi\int g(\omega_{E,i})|\alpha_{E,i}|^2\rho(E)\,dE \\ &= 2\pi\int g(\omega_{E,i})(\omega_{E,i}/\hbar c)^2|\mathbf{A}_0 \bullet \langle\Phi_E|\mu|\Phi_i\rangle|^2\rho(E)\,dE\,.\end{aligned}$$

Recalling that $\mathbf{E}(\mathbf{r},t) = -1/c\,\partial\mathbf{A}/\partial t = \omega/c\mathbf{A}_0\sin(\omega t - \mathbf{k}\bullet\mathbf{r})$, the magnitude of $\mathbf{A}_0$ can be replaced by that of the electric field strength $\mathbf{E}$, and this rate expression becomes

$$R = 2\pi\int g(\omega_{E,i})(1/\hbar)^2|\mathbf{E} \bullet \langle\Phi_E|\mu|\Phi_i\rangle|^2\rho(E)\,dE\,.$$

The intensity I, in photons per cm^2 per sec, is related to the electric field strength by

$$I = c|\mathbf{E}|^2/(8\pi\hbar\omega)$$

so, the rate can be written in terms of the intensity as:

$$R = 16\pi^2\int g(\omega_{E,i})I(\omega/c\hbar)|\mathbf{e} \bullet \langle\Phi_E|\mu|\Phi_i\rangle|^2\rho(E)\,dE$$

where $\mathbf{e}$ is a unit vector pointing in the direction of the electric field. The cross-section can also be written in this form as:

$$\sigma = 16\pi^2\int g(\omega_{E,i})(\omega/c\hbar)|\mathbf{e} \bullet \langle\Phi_E|\mu|\Phi_i\rangle|^2\rho(E)\,dE\,.$$

2.3. *Electronic, Vibrational and Rotational Components*

Finally, the most common way to describe the anion and neutral plus free electron wavefunctions is to write them as products of electronic ψ, vibrational χ, and rotational $D^J_{M,K}$ functions:

$$\Phi_i = \psi_i \chi_v D^J_{M,K}$$

$$\Phi_E = \psi_E \chi_{v'} D^{J'}_{M',K'}$$

and to assume that the electronic functions consist of single Slater determinant functions which differ by Φ_i having the spin-orbital ϕ_i where Φ_E has the continuum spin-orbital ϕ_E.

In the event that the electronic wavefunctions ψ_i and ψ_E possess nonzero angular momentum, it is necessary to properly combine this angular momentum with the rotational angular momentum. In the initial anion state, where the extra electron's motion is "locked" to the framework of anion, the electronic angular momentum is added, component by component, to the rotational angular momentum's components in a molecule-fixed coordinate system (usually taken to be those of the three eigenvalues of the moment of inertia tensor). For example, in the $X^2\Pi$ state of NH^- whose HOMO orbital occupancy π^3 is depicted below in Fig. 12, the electronic wavefunction has one unit of angular momentum along the N–H bond axis and zero components along the two axes perpendicular to this axis.

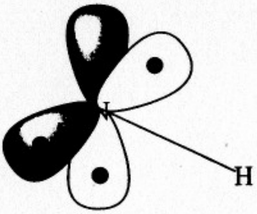

Fig. 12. HOMO orbital occupancy in the $X^2\Pi$ ground state to NH^-.

In this case, the rotational wavefunction's K quantum number (i.e. in $D^J_{M,K}$ labels the electronic function's component along the N–H axis ($K = \pm 1$).

For the neutral plus free electron state Φ_E in which the ejected electron carries away nonzero angular momentum (i.e. is ejected in a p-, d-, f-, or higher wave), it is more proper to vector couple this electron's angular momentum to the rotational angular momentum of the neutral molecule. Vector coupling is appropriate because the ejected electron's motion is no longer "locked" to the molecular framework. Thus, in such cases, the wavefunction Φ_E is replaced by a function of the form:

$$\Phi_E(J,M,K;N,L) = \Sigma_{m,M'}\langle J,M|N,L,M',m\rangle \psi_E(L,m) D^N_{M',K}\,.$$

In this function, the molecule's rotational angular momentum **N** (having component M^{prime} along the laboratory-fixed z-axis and component K along its highest symmetry axis) is vector coupled, to the electronic wavefunction's angular momentum **L** (having component m along the z-axis) to give a total angular momentum **J** (with component M along z and K along the molecular axis).

Once the electronic angular momentum has been coupled to the rotational angular momentum as described above, both the anion and neutral plus free-electron states are expressed as simple products (or sums of such products) of an electronic function, a rotational function, and a vibrational function. In the following decomposition of the rate and cross-section expressions into electronic, vibrational, and rotational components, I will take Φ_i and Φ_E to be of the simple product form for simplicity, realizing that the final results should subsequently be multiplied by vector coupling coefficients (for Φ_E) and summed over m and M' quantum numbers.

With these assumptions, the electric dipole matrix element reduces to

$$\langle \Phi_E|\mu|\Phi_i\rangle = \int D^{*J'}_{M',K'} D^J_{M,K} \int \chi^*_{v'}\chi_v \langle \psi_E|\mu|\psi_i\rangle \, d\mathbf{Q} \sin\alpha \, d\alpha \, d\beta \, d\gamma\,.$$

Here, $\mathbf{Q}$ denotes all $3N-6$ of the internal (vibrational) coordinates, and α, β, and γ are the Euler angles upon which the rotational wavefunctions depend.

The electronic integral $\langle\psi_E|\mu|\psi_i\rangle$ is assumed to be relatively insensitive to geometry (actually, to vibrational distortions only; this matrix element is, of course, a vector attached to the anion's framework and thus has components directly related to α, β and γ). Therefore, $\langle\psi_E|\mu|\psi_i\rangle$ can be factored out of the integral over $d\mathbf{Q}$, thus yielding the vibrational integrals $\int \chi^*_{v'}\chi_v \, d\mathbf{Q}$ whose squares give the well known Franck–Condon factors between the anion and neutral molecule.

As noted above, $\langle\psi_E|\mu|\psi_i\rangle$ is a vector (i.e. a first-rank tensor) with components attached to the molecule's geometrical frame, while the rotational functions $D^{*J'}_{M',K'} D^J_{M,K}$ are expressed in terms of laboratory fixed coordinates (i.e. α, β, and γ describe the orientation of the molecular frame in a space-fixed frame), angular integral $\int D^{*J'}_{M',K'} D^{J}_{M,K} \langle \psi_E | \mu | \psi_i \rangle \sin\alpha \, d\alpha \, d\beta \, d\gamma$ can be carried out by first reexpressing the components of $\langle \psi_E | \mu | \psi_i \rangle$ in the laboratory-fixed frame using standard rotation matrix algebra:

$$\langle \psi_E | \mu | \psi_i \rangle_m = \Sigma_k \langle \psi_E | \mu | \psi_i \rangle_k (D^1_{m,k})^* ,$$

where m labels the components of $\langle \psi_E | \mu | \psi_i \rangle$ in the laboratory-fixed coordinate system, k labels components of $\langle \psi_E | \mu | \psi_i \rangle$ in the molecule-fixed coordinate system, and $D^1_{m,k}$ is the transformation matrix between these two coordinate systems. The resultant integral over angles is of the form

$$\int D^{*J'}_{M',K'} D^1_{m,k} D^J_{M,K} \sin\alpha \, d\alpha \, d\beta \, d\gamma$$

(with m and k ranging over -1, 0, and 1) which vanishes unless certain selection rules hold:

$$J' = J, J+1 \text{, or } J-1 \text{ (except if } J = J' = 0 \text{ for which the integral vanishes)}$$

$$M' = M + m$$

$$K' = K + k .$$

Thus, the vibrational (Franck–Condon) and rotational (selection rules on the angular momenta of the orbital from which the electron is ejected and the continuum orbital into which the electron is ejected) aspects of the photodetachment rate or cross-section expressions are the same as in conventional photoionization or electronic absorption (or emission) spectra.

2.4. *The Electronic Integral*

There are significant differences among photodetachment, photoionization, and electronic absorption spectra when the electronic transition integral $\langle \psi_E | \mu | \psi_i \rangle$ is considered in further detail. In the photodetachment case, the orbital ψ_E is not a bound-state function (but ψ_i is) but a function that describes an electron moving in the "field" of the underlying neutral molecule. As such, $\psi_E(r, \theta, \phi)$ is orthogonal to all of the occupied bound orbitals of the anion and describes an electron with kinetic energy $E = p^2/2m_e$ for large values of r. The ψ_E orbital appropriate to photodetachment is *not* of the same form as that arising in the theory of photoionization because, in the latter case, the outgoing electron experiences the long-range Coulomb potential of the daughter cation. For anion photodetachment, the ejected electron experiences no long-range potential of the form $-e^2/r$. For anions having significant dipole moments (μ), the longest range potential varies as $-\mu\cos(\theta)/2r^2$, and for non-polar molecules, the longest range potential varies as an even higher power of r. In addition, the ejected electron's orbital angular momentum L affects the form of ψ_E because it contributes the centrifugal potential $L(L+1)/2m_er^2$ to the effective potential $V_{\text{eff}}(r)$ that shapes the radial form of ψ_E.

There are, however, many similarities among the photoionization (of neutrals), photodetachment, and electronic excitation cases. For example, symmetry can be used to determine (or constrain) the symmetry of the ejected electron's wavefunction. For the electronic matrix element $\langle\psi_E|\mu|\psi_i\rangle$ to be non-vanishing, the direct product of the symmetry of the HOMO ψ_i and the components of the electric dipole operator μ (which transform as x, y, and z) determine the symmetry components of the continuum orbital ψ_E.

Let us consider two examples. The HOMO of NH^- as shown in Fig. 12 is a p-type orbital localized nearly entirely on the nitrogen atom. The direct product (actually, for such essentially atomic cases, we couple the angular momenta of the HOMO and of μ, which has $L = 1$ to determine the angular momentum of ψ_E) of the HOMO's symmetry ($L = 1$) and that of $\mu(L' = 1)$ constrains the symmetry of ψ_E to be $L = 2$, 1, or 0. This means that d-, p- and s-wave electrons will be ejected when NH^- undergoes direct photodetachment.

Figure 7 shows the HOMO of N_2^- (which actually does not exist as a stable species, but we nevertheless use it here as another example). This orbital has predominantly d-character, so the photodetached electron would be expected to possess $L = 2+1, 2$ or $2-1$ character (i.e. to come off in f-, d- and p-waves). For anions whose HOMOs are delocalized over many atomic centers, one must decompose the HOMO into various symmetry components and corresponding amplitudes and subsequently take the direct product of μ's symmetries with each of the HOMO's components to predict the symmetry components and amplitudes of the ejected electron's orbital. An especially nice treatment of such polyatomic anion symmetry analyses was made by Reed, Zimmerman, Andersen, and Brauman.[19]

In addition to being able to use symmetry or angular momentum to predict the directional characteristics (i.e. symmetries) of the ejected electron's orbital ψ_E, the kinetic energy of this electron, KE has a significant effect on the electronic dipole matrix element $\langle\psi_E|\mu|\psi_i\rangle$ and thus on the detachment rate or cross-section. The kinetic energy is determined by the energy $\hbar\omega$ of the photons and the neutral-anion detachment energy DE:

$$\mathrm{KE} = \hbar\omega - \mathrm{DE}\,.$$

Except near thresholds (which are treated more specifically in the next section), the ejected electron departs the molecular framework "promptly" (on the time scales of vibrations and rotations). As the photon frequency ω is increased, the ejected electron carries away more and more kinetic energy. Because the radial form of ψ_E varies as $\exp(ikr)$ for large r, with $\hbar^2k^2/2m_e = \mathrm{KE}$, the orbital ψ_E will be a highly oscillatory function when KE is large (specifically, large enough to make $1/k$ small compared to the dimension of the anion's HOMO). In such cases, the integral $\langle\psi_E|\mu|\psi_i\rangle$ will have a very small magnitude because ψ_E oscillates rapidly while ψ_i and μ are smoothly varying functions of r. Thus, for photon energies far above the detachment threshold, the electron is ejected with large kinetic energy, but the rate and cross-section are small because the rapid oscillation of ψ_E causes the transition matrix element $\langle\psi_E|\mu|\psi_i\rangle$ to be small.

2.5. *Threshold Forms of Cross-Sections*

When the photon energy $\hbar\omega$ is only slightly higher than the minimum energy needed to detach an electron from a particular state (electronic/vibration/rotation) of the anion and to produce a particular (electronic/vibration/rotation) state of the daughter neutral, we say that the detachment is occurring just above threshold. In both the photodetachment and photoionization cases, angular momentum considerations allow one to make important conclusions about the nature of the cross-section (or rate) as a function of the kinetic energy of the ejected electron.

As discussed earlier in Sec. 2.4, the symmetry of the anion's HOMO and that of the electric dipole operator μ limit the range of angular momentum values L that the ejected electron can assume. Among these symmetry-allowed L values, amplitude belonging to the *smallest L will dominate* the ejected electron's flux *near thresholds*. The dominance of the smallest L is a result of the pattern in angular momentum barriers (see Fig. 9) through which the electron must tunnel to detach; the smallest L value has the lowest barrier and thus the highest rate of tunneling.

The cross-section for photodetachment at energies just above a threshold and for ejection of an electron having angular momentum L and kinetic energy KE was shown by Wigner in 1948[20] to depend on these two quantities as:

$$\sigma \propto \mathrm{KE}^{L+1/2} .$$

This so-called Wigner law, which applies to photodetachment of anions but not to photoionization of neutrals (because its derivation requires that the ejected electron experience a potential varying no stronger than r^{-2} at large r), is a result of analyzing the KE-dependence of the square of the electronic transition matrix element multiplied by the translational density of states of the ejected electron $|\langle \psi_E | \mu | \psi_i \rangle|^2 \rho(\mathrm{KE})$. The density of states vary as $\mathrm{KE}^{1/2}$, and, for small values of KE, the electronic integral squared has been shown to vary as $(\mathrm{KE})^L$ for ejection of L-wave electrons.

For the NH^- and N_2^- examples used in the preceeding section for purposes of illustration, the photoejected electrons are allowed to be ejected in *s*-, *p*-, and *d*-waves (for NH^-) or in *p*-, *d*-, and *f*-waves (for N_2^-). The smallest L values for these cases are $L = 0$ (*s*-waves for NH^-) and $L = 1$ (*p* waves for N_2^-). The cross-sections should thus depend on the photon energy (or equivalently on the kinetic energy of the ejected electron) as:

$$\sigma = \mathrm{KE}^{1/2} \text{ for } \mathrm{NH}^-, \text{ and}$$

$$\sigma = \mathrm{KE}^{3/2} \text{ for } \mathrm{N}_2^- .$$

The plots of cross-section vs KE have qualitatively different shapes near the thresholds as illustrated below in Fig. 13 which is taken from the work of Engelking and Herrick.[21]

In particular the slopes $d\sigma/d(\mathrm{KE})$ as KE approaches thereshold differ drastically and can be used as diagnostics for determining the minimum L value from experimentally measured cross-sections. The slope generally has the form

$$d\sigma/d(\mathrm{KE}) = (L + 1/2)(\mathrm{KE})^{L-1/2} .$$

For *s*-wave detachment, the slope varies as $(\mathrm{KE})^{-/12}$ near threshold; thus one sees a sharp decline (with essentially infinite slope) in σ as KE approaches zero from above. In contrast, the *p*-wave cross-section approaches

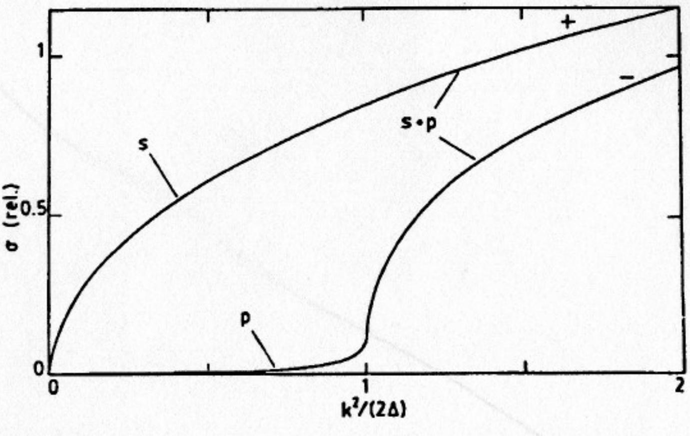

Fig. 13. Cross-sections plotted vs the kinetic energy of the ejected electron for *s*-wave and *p*-wave detachment (taken from Ref. 21). The abscissa is proportional to KE and the ordinate is proportional to the cross-section.

its threshold value (from above) with a small (zero, in principle) slope $d\sigma/d(\mathrm{KE}) = 3/2(\mathrm{KE})^{1/2}$.

Although the Wigner law analysis is very useful and remains a cornerstone for determining the symmetry of the ejected electron's orbital (and, by inference, the symmetry of the anion's HOMO), the shape of the cross-section follows this law only very close to threshold. At higher KE (or photon energy) values, corrections to this simple equation must be made.[22] The explicit form of these corrections depends on the nature of the potential experienced by the ejected electron due to the presence of the underlying neutral molecule core. In the photoionization case, the ejected electron experiences a long-range Coulomb potential which necessitates a different treatment than that used to obtain the Wigner formula. For anion photodetachment, the ejected electron can experience long-range potentials of the form (dispaying only the radial dependence) $-\mu e/r^2$ (for a molecule with dipole moment μ), $-\alpha/2r^4$ (for a molecule with polarizability α), and $-Qe/r^3$ (for a molecule with quadrupole moment Q). In practice, the magnitudes of the molecule's moments (μ, Q, and α) as well as how far above threshold one is (i.e. the KE value), combine to determine the corrections to the Wigner threshold law. A more specific consideration of these corrections is beyond the scope and level of this chapter, so it is sufficient to say that, after making such corrections, the cross-section's KE dependence can be expressed as:

$$\sigma = \sigma_0(\mathrm{KE})^{L+1/2}\{1 + a\,\mathrm{KE} + b\,\mathrm{KE}^2 + c\,\mathrm{KE}^3 + \cdots\}$$

with the correction coefficients $a, b, c, \ldots$ depending on μ, Q, α and other permanent and induced moments of the molecule.

Before closing this section it should be clarified that the Wigner threshold law presented above must be modified, even in its lowest-order (in powers of KE) term for the specific case of detaching an electron to produce a molecule having a large dipole moment.[19,22,23] In such cases, the longest-range potential experienced by the ejected electron having the smallest allowed L value varies as

$$V_{\mathrm{eff}} = L(L+1)/2m_e r^2 - \mu e \cos\theta/r^2$$

where θ is the angle between the molecule's dipole moment vector μ and the ejected electron's position vector $\mathbf{r}$. It is because both the centrifugal potential $L(L+1)/2m_e r^2$ and the longest-range electron molecule potential vary as the same power of r that this is a special case. For photoionization of neutrals (which have long-range $-e^2/r$ potentials), as mentioned earlier, a qualitatively different treatment of the threshold cross-section is needed. However, for detachment of non-polar molecules (which have zero or negligible $-\mu e \cos\theta/r^2$), the conventional Wigner law remains valid.

For the special case of detachment producing a highly polar molecule,[23] it can be shown that the cross-section near threshold varies with KE as

$$\sigma = \sigma_0(\mathrm{KE})^{\lambda+1/2}$$

where $\lambda(\lambda+1) = L(L+1) - 2m_e\mu e$ can be viewed as giving the (non-integer) effective angular momentum value λ in terms of the angular momentum L of the ejected electron and the molecule's dipole moment.

2.6. *What does One Learn from a Photodetachment Experiment?*

2.6.1. *Vibrational (and Maybe Rotational) Energy Levels of the Daughter Neutral*

For an electronically stable and geometrically stable anion, the photodetachment spectrum can be obtained in either of two ways. A fixed-energy

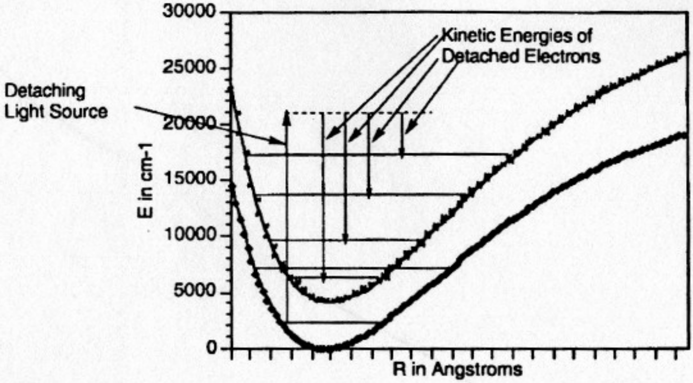

Fig. 14. Fixed frequency photodetachment of an electronically and geometrically stable anion in which the kinetic energies of the detached electrons are monitored.

light source of frequency ω can be used and the kinetic energies of the ejected electrons can be monitored. The kind of transitions probed in such an experiment are described in Fig. 14 for detachment from $v = 0$ of the anion to $v = 0$, 1, 2, and 3 of the neutral.

An example of the kind of data that arises in this kind of experiment is shown below in Fig. 15 taken from work of Leopold, Ho, and Lineberger.[24] A series of peaks corresponding to electrons ejected with differing kinetic energies are the primary data in these experiments.

In such an experiment, the electrons in the peak corresponding to the highest kinetic energies KE_0 determine the adiabatic detachment energy $\mathrm{DE}_{\mathrm{adiabatic}}$ of the anion via the energy balance equation:

$$\hbar\omega = \mathrm{KE}_0 + E_{\mathrm{anion}}(v = 0) - E_{\mathrm{neutral}}(v = 0) = \mathrm{KE}_0 + \mathrm{DE}_{\mathrm{adiabatic}}\,.$$

The energy balance equation also pertains to detachment to excited vibrational levels of the neutral:

$$\hbar\omega = \mathrm{KE}_v + E_{\mathrm{anion}}(v = 0) - E_{\mathrm{neutral}}(v)\,.$$

The spacings $\mathrm{KE}_0 - \mathrm{KE}_v$ thus provide the spacings between the neutral molecule's vibrational levels:

$$\mathrm{KE}_0 - \mathrm{KE}_v = E_{\mathrm{neutral}}(v) - E_{\mathrm{neutral}}(v = 0)\,.$$

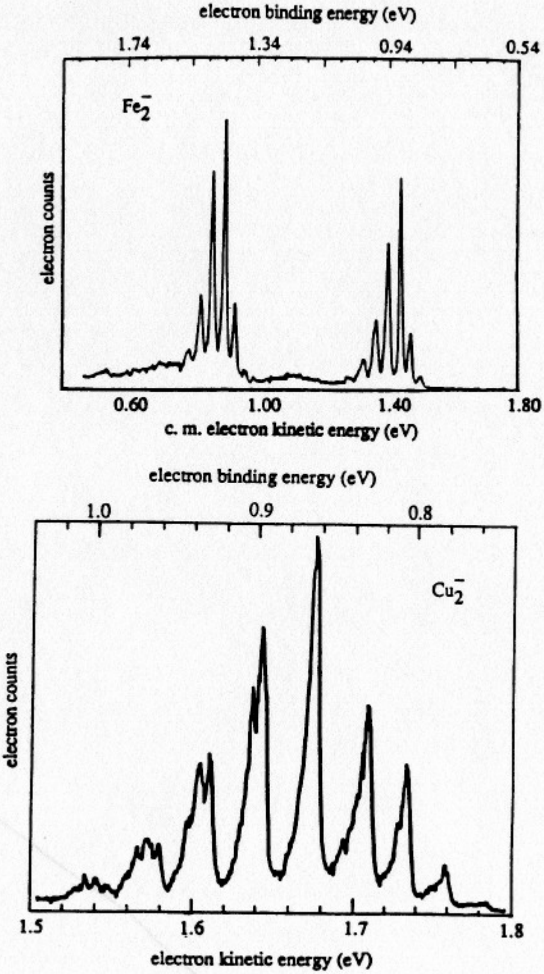

Fig. 15. Photoelectron spectrum of Fe_2^- and of Cu_2^- (taken from Ref. 24).

For the two examples cited above, these spacings give the following information:

1. The two groupings of peaks in Fe_2^- are interpreted as corresponding to transitions from $(4s\sigma)^2(4s\sigma^*)^2(3d)^{13}Fe_2^-$ to $(4s\sigma)^2(4s\sigma^*)^1(3d)^{13}Fe_2$ with the two states giving rise to the two sets of peaks corresponding to different couplings of the $(3d)^{13}$ and $(4s\sigma^*)^1$ orbitals' spins. For both sets of

peaks, removal of an electron from the $4s\sigma^*$ orbital, which is weakly antibonding, gives rise to a slight change in Fe–Fe bond length (i.e. the anion has a slightly longer bond than the neutral) and thus to a Franck–Condon vibrational progression (i.e. the individual peaks within each group) from which the vibrational spacing of 300 cm^{-1} in neutral Fe_2 can be inferred.

2. For Cu_2^-, one vibrational progression is observed with spacings of ca. 265 cm^{-1}, which is the vibrational frequency of neutral Cu_2. The shape of the Franck–Condon envelope can be explained in terms of Cu_2^- having a slightly longer bond length than neutral Cu_2 (2.345 Å compared to 2.220 Å), all of which is consistent with Cu_2 having a $(4s\sigma)^2(4s\sigma^*)^0(3d)^{20}$ orbital occupancy and Cu_2^- having $(4s\sigma)^2(4s\sigma^*)^1(3d)^{20}$ as its configuration.

The intensities of each peak are determined, as discussed earlier in Sec. 2.3, by Franck–Condon factors connecting the anion and neutral vibrational levels as well as by the squared modulus of the electronic integral $|\langle\psi_E|\mu|\psi_i\rangle|^2$ and the density of states of the ejected electrons ρ. For those peaks belonging to electrons ejected with high kinetic energy, the $|\langle\psi_E|\mu|\psi_i\rangle|^2$ factor attenuates the peak intensity because ψ_E is a highly oscillatory function of r, while peaks belonging to electrons with lower kinetic energies have intensities less attenuated. For these reasons, it is difficult to extract from the pattern of peak intensities quantitative information about the geometry differences between the anion and neutral (i.e. by using the Franck–Condon profile alone), although, as illustrated in the preceeding discussion of Fe_2^- and Cu_2^-, it is possible to glean vibrational spacing information and to estimate anion–neutral bond length changes.

Finally, if the resolution of the electron kinetic energy measurement is high enough to detect peaks with rotational structure, the spacings among such peaks can be used to determine rotational energy levels of the neutral molecule (and thus moment of inertia data). Moreover, if the anion sample is warm enough to allow other than its lowest vibrational level to be populated, hot bands may occur, for which the energy balance equation reads:

$$\hbar\omega = \text{KE}_{v'v} + E_{\text{anion}}(v) - E_{\text{neutral}}(v')$$

where v is the quantum number of the anion's vibrational level and v' is the quantum number of the neutral's level.

An alternative experiment involves the use of a light source whose frequency is scanned and the rate of appearance of ejected electrons is monitored as a function of ω (but their kinetic energies are not measured).

In such experiments, one also observes a series of peaks than can be used to determine the anion's adiabatic detachment energy and whose spacings can be used to extract the neutral's vibrational (and perhaps rotational) energy level patterns. Again, the intensities of the peaks seen in this kind of experiment depend on Franck–Condon type factors as well as the squares of electronic matrix elements and densities of states. One strength of the scanning frequency method is that one can more easily examine the near-threshold behavior of the cross-section (i.e. how the cross-section depends on the kinetic energy of the ejected electron). As discussed in Sec. 2.5, the dependence of this cross-section on KE can offer information about the angular momentum carried away by the electron and thus on the symmetry of the anion's HOMO. To study such near-threshold behavior using the scanning (photodetachment) technique is more readily achieved than within the photoelectron spectroscopy method simply because the energy resolution with which one can fix the (laser) light source energy is higher than that with which one can measure the kinetic energy of the ejected electrons.

Three examples of using threshold cross-section shapes to determine HOMO orbital symmetries are shown below in Fig. 16.

The OH^- data[25] clearly show the sharp onset charactistic of $KE^{1/2}$ behavior suggesting that the ejected electron is produced in an $L = 0$ s-wave. Therefore, one can infer that the HOMO must be of p character; indeed the OH^- HOMO is localized largely on the O atom and is of $2p_\pi$ character. In contrast, the O_2^- cross-section[26] rises as $KE^{3/2}$ suggesting ejection of a p-wave electron. This means that the HOMO of O_2^- could be of s, p, or d character; it is now known that this HOMO is the π_g^* orbital consisting of the anti-bonding combination of $2p_\pi$ orbital on the two O atoms. Finally, the NH_2^- cross-section again displays s-wave shape suggesting that the NH_2^- HOMO has p character; in fact, this HOMO is the non-bonding $2p$ orbital localized nearly fully on the N atom.

2.6.2. *Transition-Region Dynamical Information*

In recent years it has been shown that transition regions on the ground (or low-lying) electronic state surfaces of neutral species undergoing chemical reaction can be probed by photodetaching from a locally geometrically stable and electronically stable structure of the corresponding anion species. For example, Dan Neumark's group at Berkeley used photodetachment of

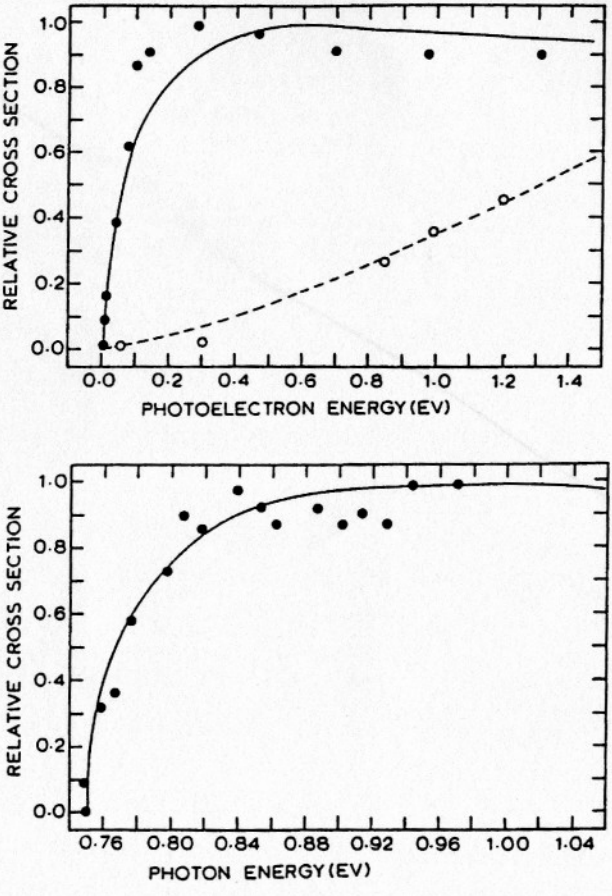

Fig. 16. Photoelectron spectra of OH^- and O_2^- (upper) and of NH_2^- (lower) very close to their respective detachment thresholds (taken from Refs. 25 and 26).

the F^-H–H van der Waals complex,[27] whose equilibrium structure is linear and rather close to the structure of the transition state on the neutral $F + HH \rightarrow FH + H$ reactive surface, to probe the reactive dynamics of the neutral near its transition state.

The basic idea underlying this use of photodetachment spectroscopy is illustrated below in Fig. 17 for the case of the $OH^-(H_2)$ van der Waals complex.[28] In this case, detachment of the $OH^-(H_2)$ complex places the neutral system on the reactive potential energy surface near the transition

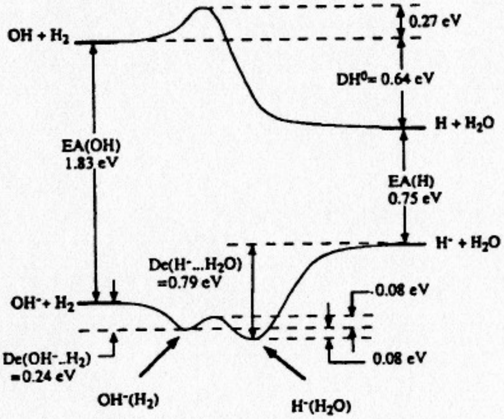

Fig. 17. Energy profiles for $OH^-(H_2)$ in relation to the $OH + H_2 \rightarrow H_2O + H$ reaction's transition state (taken from Ref. 28).

state of the $OH + H_2 \rightarrow H_2O + H$ reaction. Alternatively, detaching the $H^-(H_2O)$ van der Waals complex accesses the neutral surface far on the product side (i.e. away from the transition state near the $H_2O + H$ products).

Another example is provided in the work of Carl Lineberger's group on the photoelectron spectrum[29] of $H_2C{=}C^-$. The anion and neutral energy surfaces as functions of the CH_2 rocking normal mode are depicted in Fig. 18.

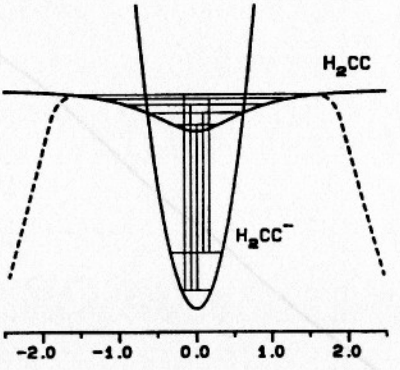

Fig. 18. Anion and neutral energy surfaces along the H_2C rocking mode (taken from Ref. 29). The barrier on the neutral surface connects $H_2C{=}C$ to HCCH.

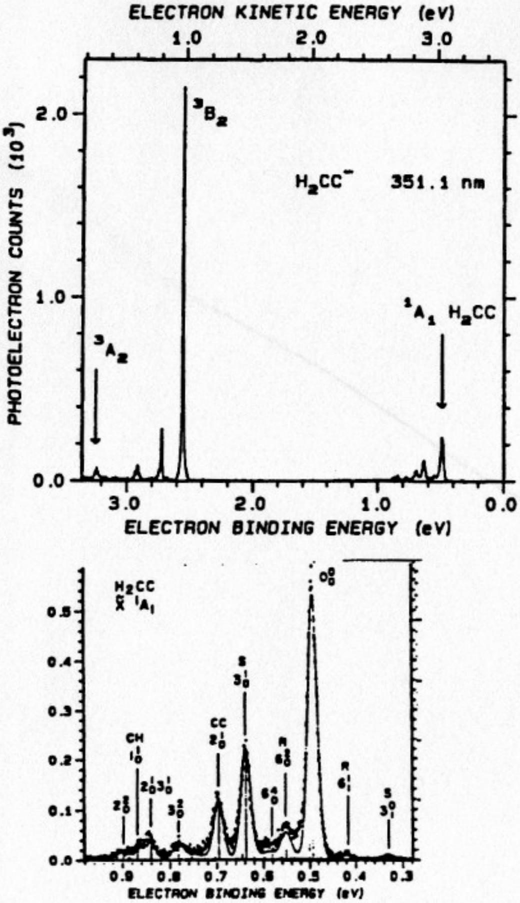

Fig. 19. Photoelectron spectrum of $H_2C{=}C^-$ (taken from Ref. 29) at low resolution (top) and, for the group of peaks belonging to the $^1A_1$ state of the neutral, at higher resolution (bottom) (taken from Ref. 29).

Because detachment of an electron from $H_2C{=}C^-$ (to produce X^1A_1 $H_2C{=}C$), especially when accompanied by excitation of the H_2C rocking mode, places the system in the region of the barrier along the X^1A_1 $H_2C{=}C$ → HCCH reaction path, the photoelectron spectrum shown in Fig. 19 has been used to extract valuable information about this transition state and to determine the energy splittings between the ground ($^1A_1$) and excited ($^3B_2$ and $^3A_2$) electronic states of $H_2C{=}C$.

It should be noted that photodetaching an anion van der Waals complex such as $F^-(H_2)$ or $OH^-(H_2)$ does not guarantee that the reactive neutral system is created at a geometry identical to the transition state geometry. However, because the anion species in the cases that have been examined is a rather tightly bound species, it has been argued that the equilibrium geometry (actually, the range of geometries accessed by vibrational motions about this equilibrium) is close enough to the geometry of the neutral's transition state that electron detachment will indeed have a reasonable Franck–Condon probability of sampling the transition state.

2.6.3. *Identification of New Molecular Anions*

One of the advantages of carrying out spectroscopies on anionic (or cationic) species is that mass selection techniques can be used to sort out complex mixtures so one knows precisely the chemical composition of the species one is examining. An example of such a study is provided by the work from Kit Bowen's laboratory at Johns Hopkins University on $H^-(NH_3)_n$ cluster anions[30] from which the photoelectron spectra shown in Fig. 20 are taken. The main peaks (labeled A and A') in $H^-(NH_3)$, and $H^-(NH_3)_2$, respectively, clearly are shifted to higher electron binding energies when compared to the unsolvated H^-, which has an electron binding energy of ca. 0.75 eV. These findings are consistent with the differential solvation of H^- compared to neutral H and with a larger solvation when two NH_3 molecules are present than when one NH_3 is used. The peaks labeled Band B' have been interpreted as due to excitation of an N–H stretching mode when one moves from the anion to the neutral; the weak intensities of these peaks have been used to conclude that the extent of N–H bond elongation is slight (thus the Franck–Condon factors are small).

What does any of this have to do with identification of new species? Although the peaks labeled A and B can straightforwardly be interpreted as belonging to an H^- ion that is "solvated" by a single intact NH_3 molecule, peak C presented a problem. This peak's intensity relative to those of peaks A and B varied from experiment to experiment, depending on specifics of the source conditions used to generate the anions. Moreover, peak C corresponds to a species having NH_4^- stoichiometry but with an electron binding energy of ca. 0.4 eV, which is considerably less even than H^-. Finally, when looked at with as high a resolution as possible, peak C seemed to consist of a single or, at most, a few vibrational sub-peaks, suggesting

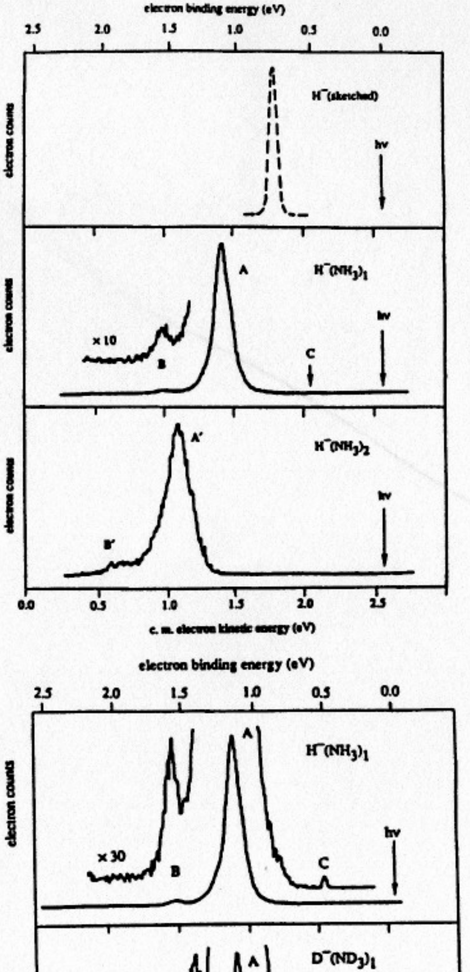

Fig. 20. Photoelectron spectra of H^-, $H^-(NH_3)$, and $H^-(NH_3)_2$ at the top and, at higher resolution for $H^-(NH_3)$ and $D^-(ND_3)$ at the bottom (taken from Ref. 30).

that whatever anion is detached in peak C, the neutral species produced has nearly the same geometry as the anion. Subsequent to the experiments in which peak C was identified, Vince Ortiz[31] carried out a series of *ab initio* theoretical calculations on an unusual isomer of NH_4^- in which the nuclear framework assumes a tetrahedral form, nearly identical to that found in the NH_4^+ cation. Ortiz interpreted the electronic nature of this isomer of the NH_4^- anion in terms of an NH_4^+ core about which a pair of electrons orbits in diffuse Rydberg-like orbitals, and his computed electron binding energy was quite close to the 0.4 eV value found in Bowen's experiments. Subsequently, other so-called double Rydberg anions[32] have been studied by other workers, but Bowen's experiments and Ortiz's calculations allowed the new species of NH_4^- to be discovered.

3. Autodetachment after Photon or Collisional Excitation

Having considered the situation in which a photon induces an *electronic transition* from the anion's HOMO to a continnum orbital relating to the neutral plus free-electron daughter, let us now consider what happens when the anion has its vibration/rotation degrees of freedom excited but does not undergo any immediate change in its electronic structure (i.e. its orbital occupancy). Figure 6 offers a pictorial representation of the kind of excitations that pertain to these cases.

It is possible for an electronically and geometrically stable anion to be promoted to an excited vibrational and/or rotational level by photon absorption or by collision with another species and for this excited anion to live as long or longer than a vibrational period. Subsequent to this excitation process, the anion can eject an electron by one of two processes. If its vibrational/rotational motions cause it to sample geometries at which the anion is no longer electronically stable (e.g. as in the $v = 2$ anion level shown in Fig. 3), an electron can detach whenever the molecular framework moves into such regions. The net rate of detachment will depend on (a) the frequency with which the anion's vibrations enter these regions of electronic instability (this, clearly, will be of the order of magnitude of the vibrational frequencies of the anion) and (b) the rate of electron detachment once the region is accessed. The latter rate will depend on whether the anion's instability is of the shape or Feshbach nature within the regions of instability. Shape resonance decay rates tend to be faster than those of Feshbach resonances with the former usually being comparable to or faster than vibrational periods. As a result, the rate limiting step (i.e. the rate that governs the ultimate rate of appearance of ejected electrons) is often the vibrational frequency for shape resonance cases and the Feshbach decay rate (attenuated by the fraction of time the anion spends in geometrical regions of instability) in these cases.

It is also possible for electron detachment to occur even if the anion and neutral energy surfaces do not cross (i.e. when the anion is not electronically unstable). If the anion's excess vibrational/rotational energy can be converted into electronic energy, an electron can be ejected with a concomitant loss of vibration/rotation energy. This kind of radiationless transition can be induced via so-called non-Born–Oppenheimer couplings as discussed in further detail below. An example of such a case is offered in Fig. 3. This particular enolate, if excited to its $v = 7, 8, 9, \ldots$ torsional vibrational level, posesses greater *total* (i.e. electronic plus vibrational) energy than the $v = 0$ level of the neutral daughter radical. However, at no geometry does the *electronic* energy of an anion cross that of the neutral, so purely electronic mechanisms for ejecting an electron are inoperative. On the other hand, if the anion were able to convert some of its excess torsion vibrational energy into electronic energy, electron ejection might occur. As discussed below and as expected, this intramolecular energy conversion will be most effective as the anion samples geometries where the anion–neutral electronic energy difference is small.

3.1. *Detachment through Shape or Feshbach Resonances*

A good example of detachment through a shape resonance state is offered by the CO_2^- species. The neutral CO_2 is linear in its $X^1\Sigma_g^+$ ground state, but the $X^2\Pi_u$ ground state of the anion, formed by adding an electron to the anti-bonding π_u orbital shown below in Fig. 21, has a bent equilibrium geometry and slightly elongated C–O bond lengths. The energies of CO_2 and CO_2^- and the C–O bond lengths as functions of the bending angle as obtained in recent work of Rod Bartlett's group[33] are shown in Fig. 22.

The formation of CO_2^- in a low vibrational level of the bending mode creates an anion with an equilibrium angle near 130°, where the C–O bond length is ca. 0.04 Å longer than in the neutral at this same angle. As this anion undergoes vibrational motion along its bending coordinate, it samples angles (e.g. greater than ca. 150°; see Fig. 22) where the anion energy

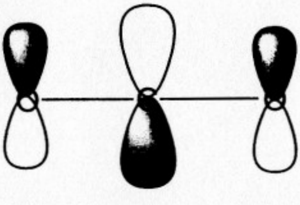

Fig. 21. The anti-bonding π_u orbital of CO_2 into which an electron is attached to form the ground state of CO_2^-.

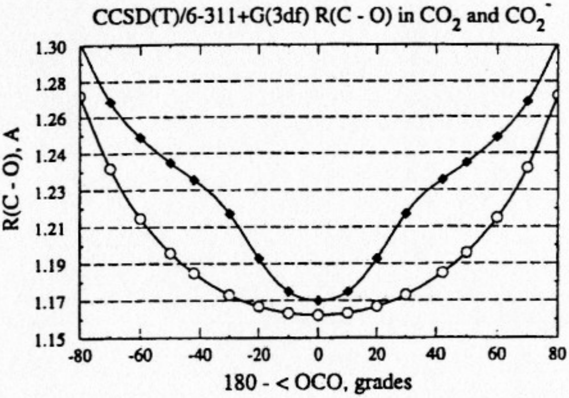

Fig. 22. Energies of ground state CO_2 (open circles) and CO_2^- (filled circles) and C–O bond lengths in the neutral (open circles) and anion (closed circles) as functions of the O–C–O bending angle (taken from Ref. 33).

lies above that of the neutral. Within these regions of anion instability, autodetachment can occur from the π_u orbital. Because the anion and neutral electronic configurations differ only in the occupancy of this single π_u orbital, which has predominantly d and p character, this decay occurs via a shape resonance and produces both d and p wave ejected electrons (n.b. we do not use the optical selection rules $L_{\text{ejected}} = L_{\text{HOMO}} \pm 1, 0$ in this case but $L_{\text{ejected}} = L_{\text{HOMO}}$ because no photon appears in the process).

Even when CO_2^- is formed by electron scattering from neutral CO_2, in which case the anion is created directly in a region (near linear geometry) where the anion curve lies above the neutral, the anion lives long enough to observe vibrational structure in a plot of the transmitted current of electrons vs electron kinetic energy such as is shown[34] in Fig. 23. In this electron transmission data, the spacings between the peaks (ca. 1113 cm^{-1})

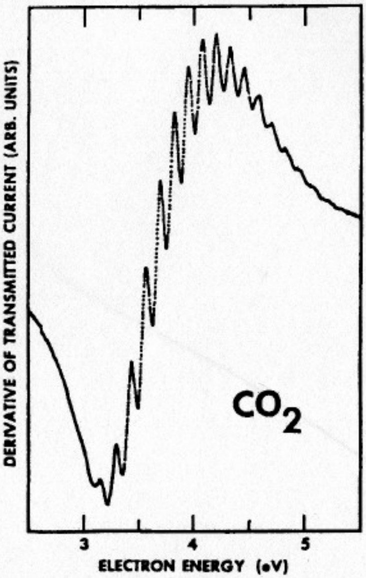

Fig. 23. Transmitted electron current vs kinetic energy of transmitted electron for scattering of electrons from CO_2 (taken from Ref. 34).

corresponds to the symmetric stretch vibrational mode. Structure belonging to the lower frequency bending mode is not seen because the lifetime of this shape resonance state (ca. 2×10^{-14} s) is shorter than the period for this slow bending motion to occur.

3.2. *Detachment through Non-Born–Oppenheimer Coupling*

3.2.1. *What are Non-Born–Oppenheimer Couplings?*

Within the Born–Oppenheimer approximation, the electronic Schrödinger equation

$$h_e(r|Q)\psi_k(r|Q) = E_k(Q)\psi_k(r|Q)$$

is solved to obtain electronic wavefunctions $\psi_k(r|Q)$, which are functions of the molecule's electronic coordinates (collectively denoted r) and atomic coordinates (denoted Q), and the corresponding electronic energies $E_k(Q)$, which are functions of the Q coordinates. The electronic Hamiltonian

$$h_e(r|Q) = \Sigma_i\{-\hbar^2/2m_e\nabla_i^2 + 1/2\Sigma_{j\neq i}e^2/r_{i,j} - \Sigma_a Z_a e^2/r_{i,a}\}$$
$$+ 1/2\Sigma_{a\neq b}Z_a Z_b e^2/R_{a,b}$$

contains, respectively, the sum of the kinetic energies of the electrons, the electron–electron repulsion, the electron–nuclear Coulomb attraction, and the nuclear–nuclear repulsion energy.

Given the solutions to the electronic Schrödinger equation, the solutions of the full Schrödinger equation (i.e. the equation in which all nuclei and electrons are moving)

$$H(r|Q)\Psi(r,Q) = E\Psi(r,Q)$$

are expressed as sums over the (complete set of functions of the electronic coordinates r) electronic functions $\{\psi_k(r|Q)\}$

$$\Psi(r,Q) = \Sigma_k \psi_k(r|Q)\chi_k(Q)$$

with the $\chi_k(Q)$ carrying the remaining Q-dependence. When substituted into the full Schrödinger equation

$$(H - E)\Sigma_k \psi_k(r|Q)\chi_k(Q) = 0$$

then using the fact that the full Hamiltonian H is h_e plus the kinetic energy operator for nuclear motion T

$$H = h_e + T = h_e + \Sigma_a(-\hbar^2/2m_a \nabla_a^2)\,,$$

premultiplying the above Schrödinger equation by ψ_n and integrating over the electronic coordinates gives the set of coupled equations that need to be solved for the $\{\chi_k\}$:

$$\begin{aligned}
&\Sigma_k \int \psi_n^*(r|Q)\{h_e + T - E\}\psi_k(r|Q)\chi_k(Q)\,dr \\
&\quad = \{E_n(Q) - E\}\chi_n(Q) + T\chi_n(Q) \\
&\qquad + \Sigma_a \Sigma_k \left\{ \int \psi_n^*(r|Q)(-i\hbar\partial\psi_k/\partial R_a)(-i\hbar\partial\chi_k/\partial R_a)/m_a\,dr \right. \\
&\qquad \left. + \int \psi_n^*(r|Q)(-\hbar^2\partial^2\psi_k/\partial R_a^2)/2m_a\,dr\,\chi_k \right\} = 0\,.
\end{aligned}$$

The expression

$$\{E_n(Q) - E\}\chi_n(Q) + T\chi_n(Q) = 0$$

is the equation governing the nuclear motion functions $\{\chi_{k,L}(Q)\}$ in the absence of the *non-Born–Oppenheimer* (*non-BO*) *coupling terms* (i.e. the two terms involving $\partial\psi_k/\partial R_a$ and $\partial^2\psi_k/\partial R_a^2$). Within this model, the vibration-rotation functions $\{\chi_k(Q)\}$ of each specific electronic state labeled k are found by solving the vibration-rotation Schrödinger equation

$$\{T + E_k(Q)\}\chi_{k,L}(Q) = \varepsilon_{k,L}\chi_{k,L}(Q)\,.$$

There are a complete set of functions of Q (i.e. the $\{\chi_{k,L}\}$ for *each* electronic state k.

The two non-BO terms are treated as perturbations (not externally applied, but arising as imperfections within this model of molecular structure) that can induce transitions between unperturbed states each of which is taken to be a specific Born–Oppenheimer product state:

$$\Psi_{k,L}(r, Q) \cong \psi_k(r|Q)\chi_{k,L}(Q)\,.$$

It is reasonably well established that the non-BO coupling term involving second derivatives of the electronic wavefunction contributes less to the coupling than do the terms $(-i\hbar\partial\psi_k/\partial R_a)(-i\hbar\partial\chi_k/\partial R_a)/m_a$ having first derivatives of the electronic and vibration-rotation functions. Hence, it is only the latter terms that will be discussed further.

With this background, the rate R (sec^{-1}) of transition from a Born–Oppenheimer initial state $\Psi_i = \psi_i\chi_i$ to a final state $\Psi_f = \psi_f\chi_f$ is given, via first-order perturbation theory, as[16]:

$$R = (2\pi/\hbar)\int |\langle\chi_i|\langle\psi_i|P|\psi_f\rangle(P/\mu)\chi_f\rangle|^2\delta(\varepsilon_f + E - \varepsilon_i)\rho(E)\,dE\,.$$

Here, $\varepsilon_{i,f}$ are the vibration-rotation energies of the initial (anion) and final (neutral) states, and E denotes the kinetic energy carried away by the ejected electron (e.g. the initial state corresponds to an anion and the final state to a neutral molecule plus an ejected electron). The density ρ of translational energy states of the ejected electron is related to the kinetic energy by $\rho(E) = 4\pi m_e L^3(2m_eE)^{1/2}/\hbar^2$. We use the shorthand notation involving $P\psi P\chi/\mu$ to symbolize the action of the multidimensional derivative operators arising in the non-BO couplings:

$$(P\psi_f)(P/\mu\chi_f) = \Sigma_a(-i\hbar\partial\psi_f/\partial R_a)(-i\hbar\partial\chi_f/\partial R_a)/m_a\,,$$

where R_a runs over the cartesian coordinates (X_a, Y_a, Z_a) of the ath atom whose mass is m_a.

3.2.2. *The Nature of the Electronic Matrix Elements*

The integrals over the anion and neutral plus free-electron electronic states

$$m_{i,f} = \langle \psi_f | P | \psi_i \rangle$$

are known[16] to be large in magnitude only under special circumstances:

1. The orbital of the anion from which an electron is ejected to form the state ψ_f of the neutral (usually the anion's highest occupied molecular orbital (HOMO)) must *be strongly modulated* or affected by movement of the molecule in one or more directions (Q). That is $\partial\psi_i/\partial Q$, which appears in $P\psi_i$, must be significant or the above integral will be small.
2. The state-to-state energy gap $\varepsilon_i - \varepsilon_f$, which is equal to the energy E of the ejected electron, must not be too large; otherwise, the oscillations in the ejected electron's wavefunction ψ_f will be so rapid as to render overlap with $\partial\psi_i/\partial Q$ negligible, again making the above integral small.

Moreover, symmetry can cause $m_{i,f} = \langle \psi_f | P | \psi_i \rangle$ to vanish. In particular, if the direct product of the symmetry of ψ_i and of $\partial/\partial Q$ do not match that of ψ_f, them $m_{i,f}$ will vanish (i.e. if direct product of the HOMO's symmetry and the symmetry of the vibration or rotation motion from which energy is transferred determines the symmetry of the ejected electron's continuum orbital).

The derivatives (i.e. the dynamic responses) of the anion's orbitals to nuclear motions $\partial\psi_i/\partial Q$ arise from two sources:

1. The orbital's LCAO-MO coefficients depend on the positions of the atoms (or, equivalently, on the anion's bond lengths and internal angles). For example, the π^* orbital of an olefin anion that contains the "extra" electron is affected by stretching or twisting the C–C bond involving this orbital because the LCAO-MO coefficients depend on the bond length and twist angle. As the bond stretches or twists, the π^* orbital's LCAO-MO coefficients vary, as a result of which the orbital's energy, radial extent, and other properties also vary.

The atomic orbitals (AO) themselves dynamically respond to the motions of the atomic centers. For example, vibration of the $X^2\Pi$ NH$^-$ anion's H bond induces d_π character into the $2p_\pi$ orbital containing the extra

$d\Psi/dR = (\Psi(R+\delta) - \Psi(R))/\delta$ causes $2p_x$ to acquire d character

$d\Psi/d\theta = (\Psi(\theta+\delta) - \Psi(\theta))/\delta$ causes $2p_x$ to acquire $2p_z$ character

Fig. 24. Responses of the NH^- $2p_\pi$ orbital to vibrational motion (left) and to rotational motion (right).

electron as shown in Fig. 24. Alternatively, rotation of this anion's N–H bond axis causes the $2p_\pi$ HOMO to acquire some $2p_\sigma$ character (see Fig. 24 again).

In summary, for non-BO coupling to be significant[16] the *anion's HOMO must be strongly modulated* by a motion (vibration or rotation) of the molecule's nuclear framework and *the state-to-state energy gap must not be too large* as to render the HOMO-to-continuum-orbital overlap insignificant. For the HOMO to be strongly modulated, it is helpful if *the anion and neutral energy surfaces approach closely* (n.b. this is not the same as requiring that the state-to-state energy gap $\varepsilon_i - \varepsilon_f$ be small) at some accessible geometries.

Before considering a few specific examples of how non-BO couplings can cause electron ejection, it is important to note that there are qualitative differences between the first-order perturbation theory rate expression shown above for the non-BO case and the analogous expression for the rate of photon absorption:

$$R = (2\pi/\hbar)|\langle\chi_i\langle\psi_i|V|\psi_f\rangle\chi_f\rangle|^2\delta(\varepsilon_f - \varepsilon_i - \hbar\omega)\,.$$

In the electronic transition spectroscopy case, the perturbation (i.e. the photon's electromagnetic potential V) appears explicitly only in the $\mu_{i,f} = \langle\psi_i|V|\psi_f\rangle$ electronic matrix element because this external field is purely an electronic operator. In contrast, in the non-BO case, the perturbation involves a *product of momentum operators*, one acting on the electronic wavefunction ($P\psi_i$) and the second ($P\chi_i/\mu$) acting on the vibration/rotation wavefunction because the non-BO perturbation involves an explicit exchange of energy and momentum between the electrons and the nuclei rather than an absorption of energy and momentum from a photon. As a result, one has matrix elements of the form $\langle\chi_i|\langle\psi_i|P|\psi_f\rangle(P/\mu)\chi_f\rangle$ in the non-BO case where one finds $\langle\chi_i|\langle\psi_i|V|\psi_f\rangle|\chi_f\rangle$ in the spectroscopy case. A primary difference is that derivatives of the vibration/rotation functions appear in the former case (in $(P/\mu)\chi$) where only χ appears in the latter.

3.2.3. *A Few Examples*

3.2.3.1. *Rotational Detachment in NH⁻*

Depicted in Fig. 1 are the anion and neutral potential curves that are qualitatively illustrative of the $X^2\Pi$ NH^- case mentioned earlier. In this anion, the HOMO is a non-bonding $2p_\pi$ orbital localized almost entirely on the N atom. As such, its LCAO-MO coefficients are not strongly affected by vibration of the N–H bond (because it is a non-bonding orbital). Moreover, the anion and neutral surfaces have nearly identical R_e and ω_e values, and similar D_e values, as a result of which these two surfaces are nearly parallel to one another over a wide range of internuclear distances and are separated by ca. 0.4 eV or more than 3000 cm^{-1} at their minima.

It has been seen experimentally[10] that excitation of NH^- to the low rotational states of the $v = 1$ vibrational level (which lies above $v = 0$ NH of the neutral and thus has enough energy to eject the electron) results in very slow (e.g. ca. 10^8 sec^{-1}) electron ejection, corresponding to ca. one million vibrational periods before detachment occurs. However, excitation to high rotational levels (e.g. $N' = 40$) of $v = 1$ produces much more rapid

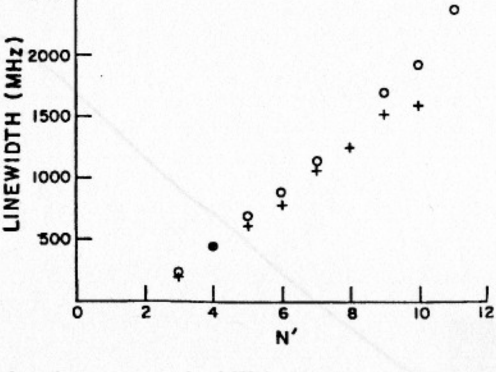

Fig. 25. Electron detachment rates (in MHz) as functions of the anion rotational level N' for transitions between NH^- $(v = 1, N')$ to NH $(v = 0$, all accessible $N) + e^-$ (taken from Ref. 10).

electron ejection (ca. 10^9–10^{10} sec^{-1}). These data, some of which are shown in Fig. 25, have been interpreted as saying that vibrational coupling is weak (i.e. $\partial\psi_i/\partial R$ is small) because of the non-bonding nature of the $2p_\pi$ MO, while rotational coupling becomes significant (i.e. $\partial\psi_i/\partial\theta$ is large) for high N'. A theoretical interpretation of these experimental findings based on the non-BO coupling theory detailed above has also been put forth.[10]

3.2.3.2. *Vibrational Detachment in Enolates*

Figure 2 shows anion and neutral potential curves, as functions of the "twist" angle of the H_2C–C bond in a typical enolate anion such as acetaldehyde enolate H_2CCHO^-. Angles near $\theta = 0$ correspond to geometries where the p_π orbital of the H_2C moiety is delocalized over the two p_π orbitals of the neighboring C and O atoms, thus forming a delocalized π HOMO. At angles near $\theta = 90°$, the p_π orbital of the H_2C group is no longer stabilizated by delocalization; so the HOMO's energy is much higher (as a result of which the anion-neutral surfaces *approach* closely). In this case, excitation of, for example, $v = 7$ in the H_2C–C torsional mode of the anion might be expected to produce electron ejection because $v = 7$ of the anion lies above $v = 0$ of the neutral. However, over the range of θ values accessible to both the $v = 7$ vibrational function of the anion and the $v = 0$ function of the neutral, the anion-neutral energy surface gap is quite large (i.e. $E_{ff}(Q) - E_i(Q)$ is large even though $\varepsilon_i - \varepsilon_f$ is small). In contrast, excitation of $v = 9$ of the anion could produce more rapid electron ejection (to $v = 2$ of the neutral, but not to $v = 0$ of the neutral) because, for the $v = 9 \rightarrow v = 2$ transition, there are angles accessed by both $v = 9$ anion and $v = 2$ neutral vibrational functions for which $E_{ff}(Q) - E_i(Q)$ is small and changing; moreover, the state-to-state gap $\varepsilon_i - \varepsilon_f$ is also small in this case.

For the particular case of the acetaldehyde enolate anion, the rates of electron ejection induced by non-BO coupling has been computed[11] for the $v = 9, 10$ and 11 levels decaying to the $v' = 0, 1, 2, 3$, and 4 levels of the neutral and found to lie between 3×10^9 s^{-1} and 7×10^{10} s^{-1}. Direct experimental probes of these state-to-state rates have not been made, but infrared multiphoton excitation of the parent enolate has been found[35,36] to produce electron ejection. These experimental findings are consistent[11] with the computed rates if one assumes that the IR excitation energy is quickly distributed among all internal vibrational modes of the anion so the probability of observing the anion in a particular torsional level v is given by the statistical density of states probability of this state.

3.2.3.3. *Collisional Detachment in OH⁻*

A third example is offered by the $O^- (^3P) + H(^2S) \rightarrow OH(X^2\Pi) + e^-$ associative electron detachment process. The pertinent anion and neutral potential energy curves[37] are shown below in Fig. 26. In this process, collisions between gas-phase O^- ions and H atoms take place on the $^1\Sigma$ and $^1\Pi$ curves (as well as on the $^3\Sigma$ and $^3\Pi$ curves which are not shown in the figure). Those collisions that begin on the $^1\Sigma$ curve have some probability of (a) coupling the H 1s electron with the O $2p_\sigma$ electron to form an intact σ bond after which (b) non-BO coupling can eject a $2p_\pi$ electron to produce $X^2\Pi$ OH $+ e^-$. In this situation, the non-BO coupling occurs between an initial $^1\Sigma$ electronic state and a continuum collisional state (rather than an initial bound vibrational state as in the earlier examples) and a final $^2\Pi + e^-$ electronic state and a bound vibrational state of OH. Because the electronic energy gap between OH^- and OH is very large (ca. 1.8 eV), the rates of these non-BO induced electron ejections are found to be extremely slow for this case (e.g. rates of the order 10^4 s^{-1} for thermal collision energies).

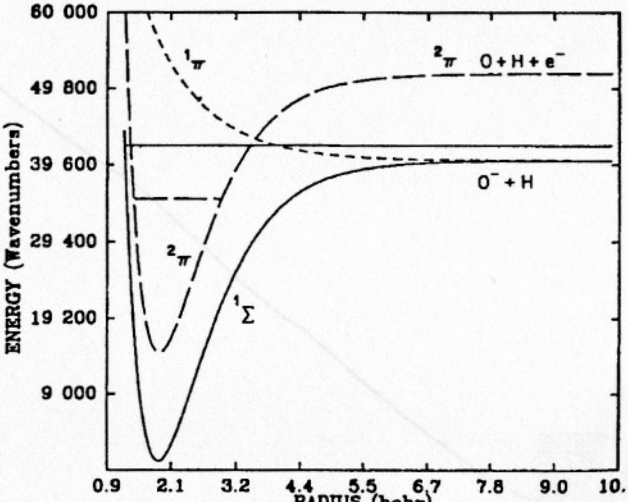

Fig. 26. Anion $^1\Sigma$ and $^1\Pi$ and neutral $^2\Pi$ energy curves for OH^- and OH, respectively (taken from Ref. 37).

3.2.3.4. *Rotational Detachment in Dipole–Bound Anions*

The neutral radicals H_2C–CN and H_2C–CHO both have large dipole moments (ca. 3.71 Debyes for the former and 3.05 Debye for the latter) and they each have an unfilled valence orbital. Therefore, both of these species can attach an electron to form:

1. a valence-bound anion state (H_2CCN^- and H_2CCHO^-) having large electron binding energy (12 500 cm^{-1} for the former and $> 14\,700$ cm^{-1} in the latter) as well as
2. an (excited) dipole-bound state in which the electron is bound very weakly to the underlying neutral radical core (< 66 cm^{-1} in the former and ca. 5 cm^{-1} in the latter).

In dipole-bound anions,[38] the "extra" electron is attracted to the underlying neutral molecule core by a variety of forces, but the potential arising from the charge-permanent dipole interaction, which has the form $-\mu e \cos\theta / r^2$, has a dominant influence and is the longest-range potential. For molecules with dipole moments in the range of 2–10 Debyes, the extra

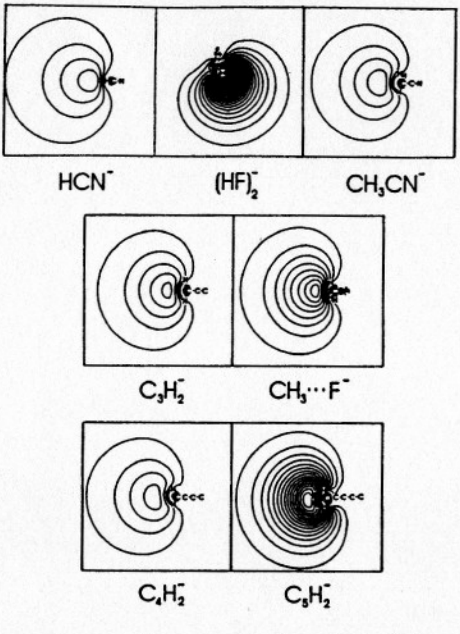

Fig. 27. Molecular structures and contour graphs of dipole-bound orbitals for several dipole-bound anions (taken from the Gutowski *et al.* article mentioned in Ref. 38).

electron is bound by a few to a few hundred cm^{-1} in such states. As a result, the orbital in which the dipole-bound electron resides is very diffuse. Several examples of these orbitals are shown in Fig. 27 in the form of contour plots overlaying the molecular structure shown to scale.

Most experiments[39,40] that probe the non-BO induced electron detachment within the dipole-bound states of these anions begin with the anions in their valence-bound electronic states and use a laser to excite a particular rotational transition from the J, M and K level of the valence-bound state to a well specified level (determined by selection rules) J', M' and K' of the dipole-bound state. The quantum numbers J, M and K refer, as usual, to the total angular momentum, its projection along a laboratory-fixed axis, and its projection along the (near) symmetry axis of the molecule.

As suggested in Fig. 28 for the H_2CCN^- case, subsequent to formation of the dipole-bound anion in a well specified rotational state, autodetachment is observed to occur producing $H_2CCN + e^-$.

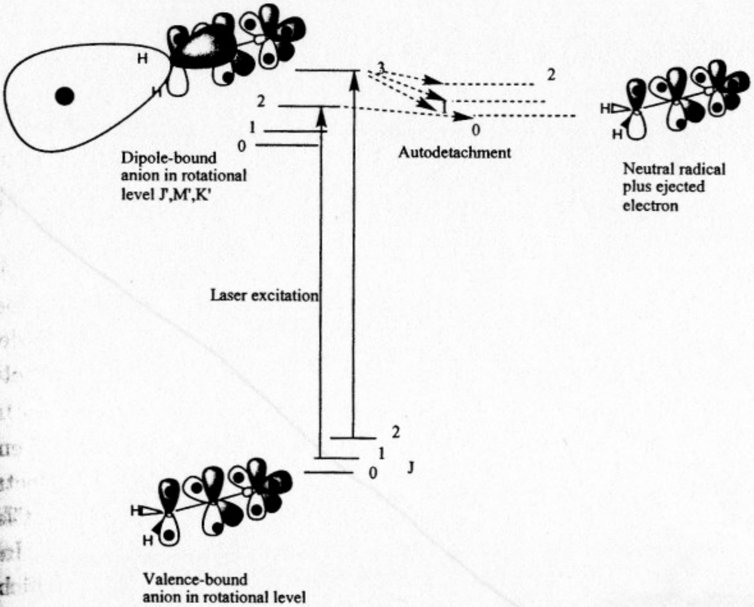

Fig. 28. Depiction of how laser excitation of the valence-bound anion H_2CCN^- to a particular rotational level of the dipole-bound state prepares the latter for subsequent autodetachment to produce $H_2CCN + e^-$.

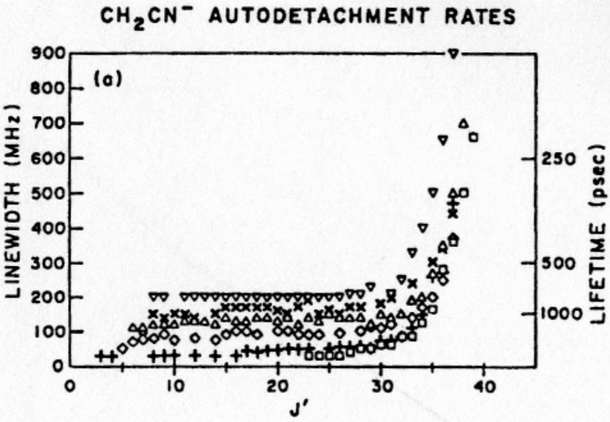

Fig. 29. Decay rates (MHz) of rotational levels of dipole-bound H_2CCN^- vs rotational quantum number J'. The various sets of data correspond to different K' values with larger K' giving only slightly higher decay rates (taken from Ref. 40).

The rate of electron ejection, as inferred by the linewidths of the photodetachment spectrum, is found to depend very strongly on the rotational energy content of the dipole-bound anion as shown below in Fig. 29. More specifically in the above example of H_2CCN^-, the rate is found to grow rapidly with J' beyond ca. $J' = 30$, but in a manner that is relatively insensitive to the component K' of rotational angular momentum along the (near) symmetry axis. This suggests that the rotational energy that does not move the dipole moment vector (i.e. spinning of the molecule about its (near) symmetry axis, which relates to the K' quantum number) is ineffective at electron detachment. Only overall tumbling motion of the molecule, and thus of the dipole moment vector, seems to cause coupling between rotational and electronic energies.

A theoretical model describing the dynamics by which rotational energy and angular momentum of the dipole-bound anion is coverted into electronic energy eventually leading to electron ejection has been presented by Clary[41] and applied to both H_2CCN^- and H_2CCHO^- with good success. In this model, the rate of electron ejection is related to the rate at which the electron moves through the classically forbidden region of an effective radial potential $W(R)$ from small R (where the electron is localized in the dipole-bound orbital and the molecule has rotational quantum number J) to larger and larger R (where the molecule loses angular momentum as the electron

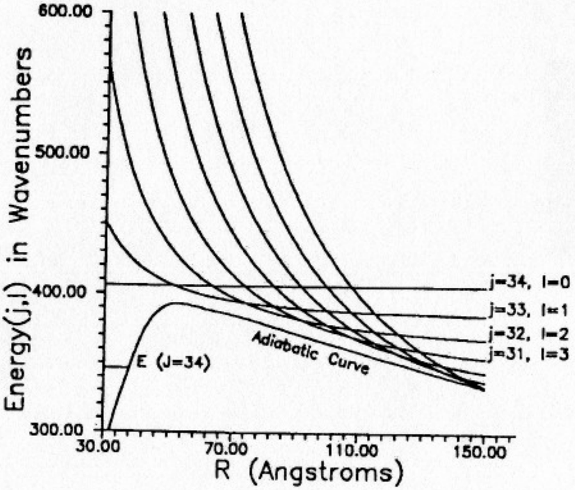

Fig. 30. Effective radial potential (smooth lower curve) arising for $J = 34$ in the case of dipole-bound H_2CCN^-. Also shown are the various j, L components that form the smooth adiabiatic radial potential (taken from the Simons article in Ref. 41).

gains energy and angular momentum), eventually producing the ejected electron with angular momentum L and the neutral molecule with $j < J$. An example of such a radial potential and the J, j, and L values that pertain to $J = 34$ is shown in Fig. 30.

4. Summary

In this chapter, I have tried to both give an overview of the theoretical underpinnings that allow experimental data (e.g. photodetachment or photoelectron rates or cross-sections or electron detachment rates for excited vibration/rotation/translation states of electronically stable anions) to be intepreted in terms of the orbitals and nuclear motion states of the parent anion and daughter neutral species. By defining the various kinds of stability that an anion may possess, I tried to make it clear what kind of species were to be included in (and what kind are excluded from) my discussion. By separating direct photon-induced detachment from other processes, I tried to make distinct the discussions of inherently electronic transitions (i.e. those in which the photon changes the anion's electronic orbital occupancy) and electron detachment induced by nuclear motions either causing the anion to sample geometries where the anion undergoes spontaneous electron loss or inducing detachment via non-BO internal energy transfer). Finally, I tried to integrate into the discussion examples, taken from the experiences of several of the leading experimental groups who study anion detachment, of the various electron detachment processes that I have treated in this chapter. By so doing, I hoped to make clear what one learns from such experimental data and why carrying out experimental and theoretical research on molecular anions and their diverse electron detachment mechanisms is challenging, exciting to puruse, and filled with important new insights yet to be gained.

Acknowledgments

This work has been supported by NSF Grant CHE-9618904 and by proceeds of the Henry Eyring Endowed Chair.

References

1. G. J. Schultz, *Rev. Mod. Phys.* **45**, 423 (1973).
2. R. S. Berry, *Chem. Rev.* **69**, 533 (1969).
3. K. D. Jordan and P. D. Burrow, *Acc. Chem. Res.* **11**, 341 (1978).
4. J. Kalcher, Annual Reports, *The Royal Society of Chemistry*, Section **C93**, 147 (1995).
5. J. Simons and K. D. Jordan, *Chem. Rev.* **87**, 535 (1987).
6. M. K. Scheller, R. N. Compton and L. S. Cederbaum, *Science* **270**, 1160 (1995).
7. B. K. Janousek and J. I. Brauman, In *Gas Phase Ion Chemistry* **2**, Ed. M. T. Bowers (Academic Press, New York, 1979).
8. H. Hotop and W. C. Lineberger, *J. Phys. Chem. Ref. Data* **14**, 731 (1985).
9. R. N. Compton, In *Negative Ions*, Ed. V. A. Esaulov (Cambridge Univ. Press, 1995).
10. The experimental findings on this anion are detailed in D. M. Neumark, K. R. Lykke, T. Andersen and W. C. Lineberger, *J. Chem. Phys.* **83**, 4364 (1985). Theoretical analysis of this same species appears in G. Chalasinski, R. A. Kendall, H. Taylor and J. Simons, *J. Phys. Chem.* **92**, 3086 (1988).
11. An experimental study on enolates is give in A. H. Zimmerman, K. J. Reed and J. I. Brauman, *J. Am. Chem. Soc.* **99**, 7203 (1977). A theoretical study pertinent to the acetaldehyde enolate system appears in D. O'Neal and J. Simons, *J. Phys. Chem.* **93**, 58 (1989).
12. This particular dianion was examined in H. G. Weikert, L. S. Cederbaum, F. Tarantelli and A. I. Boldyrev, *Z. Phys.* **D18**, 299 (1991). This energy profile was produced in A. I. Boldyrev, M. Gutowski and J Simons, *Acc. Chem. Res.* **29**, 497 (1996).

13. See the chapter in this book by Nora Berrah.
14. J. I. Steinfeld, *Molecules and Radiation* (MIT Press, 1981).
15. P. F. Bernath, *Spectra of Atoms and Molecules* (Oxford Univ. Press, New York, 1995).
16. The theory of such radiationless transitions has been treated (for autoionization of Rydberg states of neutral molecules) in R. S. Berry, *J. Chem. Phys.* **45**, 1228 (1966). This theory has been extended to non-BO induced autodetachment in molecular anions in J. Simons, *J. Am. Chem. Soc.* **103**, 3971 (1981).
17. Good discussions of the differences between shape and Feshbach resonances are contained in Ref. 1 and in H. S. W. Massey, *Negative Ions, 3rd ed.* (Cambridge Univ. Press, New York, 1976).
18. This development follows that found in several text books on molecular spectroscopy including: *Quantum Mechanics in Chemistry*, J. Simons and J. Nichols (Oxford University Press, 1997).
19. K. J. Reed, A. H. Zimmerman, H. C. Andersen and J. I. Brauman, *J. Chem. Phys.* **64**, 1368 (1976).
20. E. P. Wigner, *Phys. Rev.* **73**, 1002 (1948).
21. P. C. Engelking and D. R. Herrick, *Phys. Rev.* **A29**, 2425 (1984).
22. A good treatment of such corrections and of the origins of the Wigner law itself can be found in T. F. O'Malley, *Phys. Rev.* **137**, A1668 (1965).
23. Other good sources of further information about corrections to the Wigner law, to the inclusion of long-range electron-dipole interactions, and to the use of symmetry in polyatomic anions include: R. D. Mead, K. R. Lykke and W. C. Lineberger, *Electronic and Atomic Collisions*, Eds. J. Eichler, I. V. Hertel and N. Stolterfoht (Elsevier, Science, Publishers) see also Ref. 22; D. R. Herrick and P. C. Engleking, *Phys. Rev.* **A4**, 2421 (1984) p. 721.
24. The photoelectron spectrum of Fe_2^- is examined in D. G. Leopold and W. C. Lineberger, *J. Chem. Phys.* **85**, 51 (1986). That of Cu_2^- is covered in D. G. J. Ho and W. C. Lineberger, *J. Chem. Phys.* **86**, 1715 (1987).
25. L. M. Branscomb, *Phys. Rev.* **148**, 11 (1966).
26. S. Burch, S. J. Smith and L. M. Branscomb, *Phys. Rev.* **112**, 171 (1958).
27. S. E. Bradforth, D. W. Arnold, D. M. Neumark and D. E. Manolopoulos, *J. Chem. Phys.* **99**, 6345 (1993).
28. E. de Beer, E. H. Kim and D. M. Neumark, *J. Phys. Chem.* **99**, 13627 (1995).
29. K. M. Ervin, J. Ho and W. C. Lineberger, *J. Chem. Phys.* **91**, 5974 (1989).
30. K. H. Bowen and J. G. Eaton, in *Proceedings of the International Workshop on the Structure of Small Molecules and Ions*, Jerusalem, Israel; S. T. Arnold, J. G. Eaton, D. Patel-Misra, H. W. Sarkas and K. H. Bowen, in *Ion and Cluster Ion Spectroscopy and Structure*, Ed. J. P. Maier (Elsevier, New York, 1989).
31. J. V. Ortiz, *J. Chem. Phys.* **87**, 3557 (1987).
32. J. Simons and M. Gutowski, *Chem. Rev.* **91**, 669 (1991).
33. G. L. Gutsev, R. J. Bartlett and R. N Compton, *J. Chem. Phys.* **108**, 6756 (1998).

34. L. Sanche and G. J. Schulz, *J. Chem. Phys.* **58**, 481 (1973).
35. C. A. Wight and J. L. Beauchamp, *J. Am. Chem. Soc.* **103**, 6501 (1981).
36. R. N. Rosenfeld, J. M. Jasinski and J. I. Brauman, *J. Chem. Phys.* **71**, 1030 (1979).
37. P. K. Acharya, R. A. Kendall and J. Simons, *J. Chem. Phys.* **83**, 3888 (1985).
38. A good overview of recent theoretical work on the electronic structures of dipole-bound anions is given in M. Gutowski, K. D. Jordan and P. Skurski, *J. Phys. Chem.* **A102**, 2624 (1998). An earlier overview is given in K. D. Jordan, *Acc. Chem. Res.* **12**, 36 (1979).
39. R. D. Mead, K. R. Lykke, W. C. Lineberger, J. I. Marks and J. I. Brauman, *J. Chem. Phys.* **81**, 4883 (1984).
40. K. R. Lykke, D. M. Neumark, T. Andersen, V. J. Trapa and W. C. Lineberger, *J. Chem. Phys.* **87**, 6842 (1987).
41. D. C. Clary, *J. Phys. Chem.* **92**, 3173 (1988). Also, see J. Simons, *J. Chem. Phys.* **91**, 6858 (1989).